scientific reports

Check for updates

OPEN

Arthroscopic device with bendable tip for the controlled extrusion of hydrogels on cartilage defects

Daniele Guarnera[1,2]✉, Francesco Restaino[1,2], Lorenzo Vannozzi[1,2], Diego Trucco[1,2,3], Tommaso Mazzocchi[4], Michał Worwąg[5], Tomasz Gapinski[6], Gina Lisignoli[3], Stefano Zaffagnini[7], Alessandro Russo[7] & Leonardo Ricotti[1,2]

Advanced tools for the in situ treatment of articular cartilage lesions are attracting a growing interest in both surgery and bioengineering communities. The interest is particularly high concerning the delivery of cell-laden hydrogels. The tools currently available in the state-of-the-art hardly find an effective compromise between treatment accuracy and invasiveness. This paper presents a novel arthroscopic device provided with a bendable tip for the controlled extrusion of cell-laden hydrogels. The device consists of a handheld extruder and a supply unit that allows the extrusion of hydrogels. The extruder is equipped with a disposable, bendable nitinol tip (diameter: 4 mm, length: 92 mm, maximum bending angle: 90°) that guarantees access to hard-to-reach areas of the joint, which are difficult to get to, with conventional arthroscopic instruments. The tip accommodates a biocompatible polymer tube that is directly connected to the cartridge containing the hydrogel, whose plunger is actuated by a volumetric or pneumatic supply unit (both tested, in this study). Three different chondrocyte-laden hydrogels (RGD-modified Vitrogel®, methacrylated gellan gum, and an alginate–gelatine blend) were considered. First, the performance of the device in terms of resolution in hydrogel delivery was assessed, finding values in the range between 4 and 102 µL, with better performance found for the pneumatic supply unit and no significant differences between straight tip and bent tip conditions. Finite element simulations suggested that the shear stresses and pressure levels generated during the extrusion process were compatible with a safe deposition of the hydrogels. Biological analyses confirmed a high chondrocyte viability over a 7-day period after the extrusion of the three cell-laden hydrogel types, with no differences between the two supply units. The arthroscopic device was finally tested ex vivo by nine orthopedic surgeons on human cadaver knees. The device allowed surgeons to easily deliver hydrogels even in hard-to-reach cartilage areas. The outcomes of a questionnaire completed by the surgeons demonstrated a high usability of the device, with an overall preference for the pneumatic supply unit. Our findings provide evidence supporting the future arthroscopic device translation in pre-clinical and clinical scenarios, dealing with osteoarticular treatments.

Finding an effective treatment for articular cartilage defects due to traumas or degenerative pathologies still represents a challenge, at present[1]. Over the last decades, three-dimensional (3D) printing has targeted the design of constructs mimicking the complexity of the cartilage, to replace the damaged tissue[2,3]. In vitro bioprinting needs to define a priori the desired volume and shape through computed tomography or magnetic resonance imaging scans. Normally, in vitro maturation of the construct can take several weeks, posing limitations in the clinical translation[4]. Often, ex situ-printed constructs risk not to fit the site of interest once implanted (e.g., due to swelling or deformation)[5]. These issues, together with an increased risk of contamination due to transportation, manual implantation, and suturing, are delaying a broad application of ex situ-printed constructs in the clinics.

[1]The BioRobotics Institute, Scuola Superiore Sant'Anna, Piazza Martiri della Liberta' 33, 56127 Pisa, Italy. [2]Department of Excellence in Robotics and AI, Scuola Superiore Sant'Anna, Piazza Martiri della Liberta' 33, 56127 Pisa, Italy. [3]IRCCS Istituto Ortopedico Rizzoli, SC Laboratorio di Immunoreumatologia e Rigenerazione Tissutale, Via di Barbiano, 1/10, 40136 Bologna, Italy. [4]Relief S.R.L, Viale Rinaldo Piaggio 32, 56025 Pontedera, Italy. [5]Vimex Endoscopy, Ul. Toruńska 27, 44-122 Gliwice, Poland. [6]Lega Medical Sp. Z o. O, ul. Majowa 11, 44-217 Rybnik, Poland. [7]IRCCS Istituto Ortopedico Rizzoli, Orthopaedic and Traumatologic Clinic, Via di Barbiano, 1/10, 40136 Bologna, Italy. ✉email: daniele.guarnera@santannapisa.it

These reasons encouraged the investigation of alternative paradigms, in recent years[6,7]. Intra-operative bioprinting (IOB), also known as in situ bioprinting, grounds on the deposition of a hydrogel directly into the anatomical target to reconstruct or repair the damaged tissue through a surgical procedure. This approach aims to integrate the printing and implantation phases to overcome material manipulation-related issues and reduce the overall procedure time[8,9]. Among the IOB strategies pursued recently, the extrusion-based approach represents the most versatile one, due to low cost, high efficiency, and flexibility when the fabrication of complex constructs is targeted. In extrusion-based systems, a cell-laden hydrogel, loaded into a cartridge, is extruded by applying relatively low pressure to the plunger. Within extrusion-based IOB, two strategies are typically pursued, based respectively on: (1) robotic arms, and (2) handheld extrusion devices.

In the former case, a bioprinting unit is mounted on the end effector of a robotic arm. The architecture of the implant is designed via computer-aided design software, and the robotic arm is controlled by defining motion planning, considering the position of the anatomical structures. This solution guarantees the rapid fabrication of complex structures with high accuracy due to the minimization of human errors. Despite a high potential, the robotic arm bulkiness restricts the application of these technologies to superficial tissues, such as the skin; open surgery scenarios are required to effectively treat internal organs or tissues, such as bone, cartilage, and muscle[10–12].

In the latter case, a handheld delivery device allows manual control of the hydrogel deposition on the site of interest. This approach has several advantages, such as increased freedom to operate for the surgeon, portability, ease of sterilization, and low cost. An interesting example of a handheld extrusion device is the *Biopen*[13,14] proposed for the treatment of cartilage defects in a direct-write fashion way. In recent years, other examples of handheld delivery devices have been developed, as reviewed by Zhao and colleagues[15]. A handheld skin printer was proposed by Hakimi et al.[16], enabling the formation of skin tissue sheets with different compositions. Such an instrument was thought to be manually positioned on the target surface site, and deposit biomaterials by exploiting a microfluidic cartridge. In other papers, partially automated handheld extruders have been proposed, aiming at locally depositing composite biomaterials able to assist bone reconstruction or to treat volumetric muscle loss[17,18].

One of the main disadvantages of the handheld delivery devices available in the state-of-the-art is their inability to treat hard-to-reach sites within complex environments (e.g., the knee joints) through a minimally invasive approach. For this purpose, the device's dexterity must be improved. Adding further degrees of freedom to the tip (i.e., tip bending), together with the miniaturization of the cannula to fit minimally invasive procedures, would be a key to effectively accessing remote areas that are arduous to treat, with conventional instruments.

In this work, a novel handheld delivery device for the controlled extrusion of cell-laden hydrogels in an arthroscopic scenario is presented. The handheld extruder is supplied by an external unit and allows to bend the tip up to 90°, to reach even the most remote lesions of the knee cartilage. The device can extrude a wide range of cell-laden hydrogels with high accuracy and presents a high grade of usability.

In conclusion, the ongoing quest for effective treatments for articular cartilage defects has driven the exploration of innovative paradigms such as intra-operative bioprinting. Our work introduces a novel handheld delivery device designed to address the limitations of current approaches, offering enhanced dexterity and precision in treating challenging lesions within arthroscopic settings.

Methods

System overview

As depicted in Fig. 1, the device is composed of a handheld arthroscopic extruder and a supply unit. The handheld extruder includes a bendable tip whose hollow structure is made of nitinol, a biocompatible material featuring a *superelastic* response. The tip can be bent up to 90° around the x-axis and can also rotate (around the y-axis). The tip bending is manually controlled by the surgeon through a trigger-based mechanism, enabled by a metallic, biocompatible cable tied between the tip edge and the trigger. The tip rotation is actuated through a wheel on the handle back. The wheel rotation is transmitted to the internal rod through a connection element (transmission-bearing coupling). As a result, the rod rotation causes both cannula and tip rotation around the y-axis. The tip is mechanically tied by the cannula through a connector and can be easily removed after use to undergo sterilization. The tip hosts, internally, a low-hardness thermoplastic biocompatible polyurethane (TPU) tube, compliant with ISO 13485:2016, through which a hydrogel can be extruded. A cartridge containing the cell-laden hydrogel is housed on top of the case and it is directly connected to the supply unit, which applies pressure to the cartridge plunger for the extrusion. In this work, two different supply units were developed and compared: the former based on a motorized slider moving a fluid (water) and thus exerting a hydraulic push to the cartridge plunger (volumetric system); the latter based on a pneumatic pump, electronically controlled, which generates a pressurized air pushing the cartridge plunger (pneumatic system).

Three different hydrogels (RGD-modified Vitrogel®, VG-RGD, methacrylated gellan gum, GGMA, and alginate–gelatin blend, AG) were used to validate the device functionality.

Design and mechanical characterization of the tip

The nitinol tips were fabricated by Meko Manufacturing e.K. (Sarstedt, Germany). The tip length was set to 92 mm, while the outer diameter was equal to 4 mm. Three modules were used to bend the tip to + 90°. Each module was featured by the notch height (h = 1.7 mm) and the flap height (d = 2.1 mm). Four tip versions were evaluated, which differed for the presence of an incision (Versions B and D) and an abutment (Versions C and D), with respect to Version A. 3D Finite element (FE) analyses were performed with Abaqus 2020 (Dassault Systems, France) to assess the stress distribution for the four versions. About 200,000 linear *hex* elements were used to mesh the models uniformly, and an explicit solver was used to solve the equations.

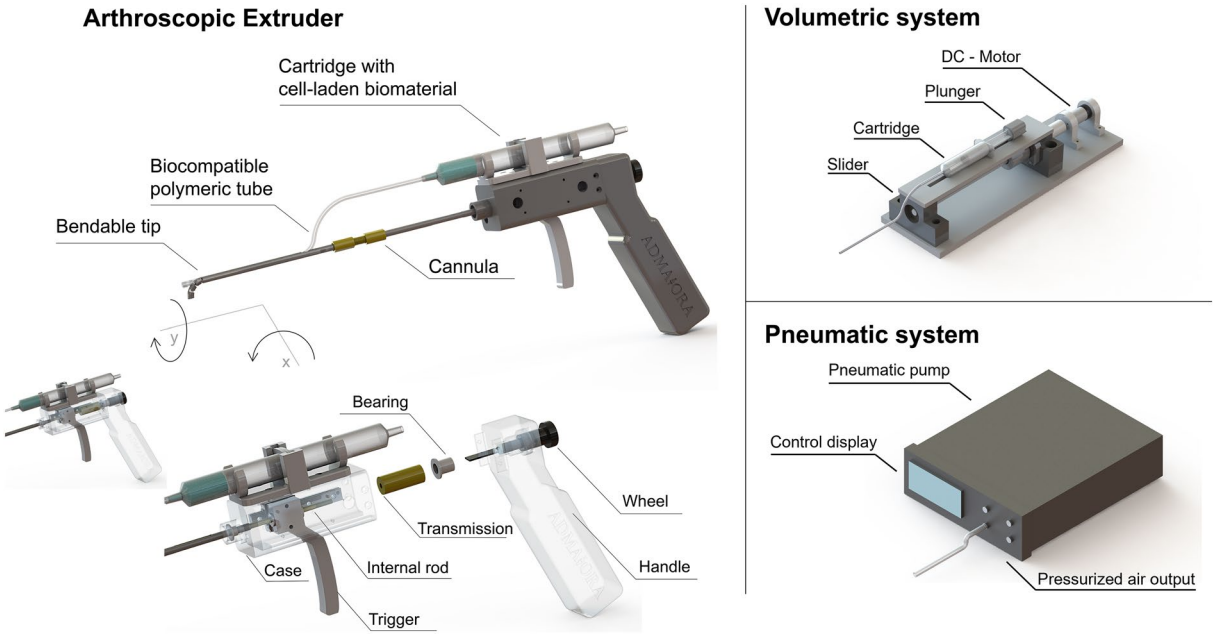

Fig. 1. Depiction of the handheld arthroscopic delivery device proposed in this work; (left): arthroscopic extruder and its main components; (right): supply units for driving a controlled hydrogel extrusion, based on volumetric (top) or pneumatic (bottom) principle.

The mechanical behavior of the tips was characterized through a Universal Testing System (model 2444, Instron, Norwood, MA, USA). Firstly, the force required to bend the tips was measured with an ad hoc setup. A cable (steel alloy AISI 316 l) was coupled to the tip and pulled imposing a displacement rate of 28 mm/min. Force values were read by a load cell (F_{max} = 10 N). The video acquired during the test (Supplementary Video S1) was processed in MatLab to correlate the bending angle with data obtained with the testing machine. The components of the setup used to bend the tip up to − 90° were developed through 3D printing. The curvature of tip versions B and D was evaluated through a digital microscope (Hirox model HRX-01, Japan). Finally, the setup used to measure the force was also used to carry out a fatigue analysis on the nitinol tip. For this purpose, the tip was subjected to 1000 flexion-release cycles with a frequency equal to 0.5 Hz (one complete flexion-release cycle every two seconds), and a vertical pulling speed equal to 7 mm/s.

Hydrogel preparation

VG-RGD was purchased from Well Bioscience (North Brunswick, NJ, USA) and prepared following the manufacturer's protocol. The VG-RGD solutions were directly mixed at room temperature (RT) with the Dilution Solution Type 1® (The Well Bioscience, North Brunswick, NJ, USA) at the ratio of 1:2. This concentration was chosen according to previously published work[19]. Culture medium (Growth Medium, GM, cod. 411-500, Cell applications, Inc) was added to the solution at the ratio of 4:1 (pre-crosslinked solution: GM) at RT.

Methacrylated gellan gum (GGMA) was obtained by performing the methacrylation procedure reported in other studies[20]. Briefly, gellan gum (GG, Gelzan®, Merck) was dissolved in deionized water (d-H_2O, 1% w/v) with a magnetic stirrer at 75 °C for 1 h. Then, the solution was cooled to 60 °C, and 8.5 mL of methacrylic anhydride (MA, Merck) per 100 mL of solution were slowly added. The solution was left reacting at a controlled pH range (8–9.5) for 6 h, then centrifuged for 3 min at 3500 rpm and at 30 °C to remove the unreacted MA. Thus, the supernatant was diluted (1:2) with d-H_2O pre-heated at 40 °C and dialyzed at 60 °C for 5 d (MWCO:12–14 kDa, Spectra/Por). Finally, aliquots were quickly frozen, lyophilized (Labconco, FreeZone 2.5 Plus) for 3 days to obtain the GGMA powder, and stored before use at − 80 °C. The GGMA powder was autoclaved at a temperature of 120 °C and a pressure of 1 bar for 30 min. Then, it was dissolved in phosphate buffer solution (PBS without Ca^{2+}/Mg^{2+}, Life Technologies) at a final concentration of 2% w/v until reaching a homogeneous solution in a water bath at 37 °C. Then, tris (2,2′-bipyridyl) ruthenium (II) chloride hexahydrate/sodium persulfate (Ru/SPS, Merck) was added and gently mixed to the solution to reach a final concentration of 0.2/2 mM, respectively. The solution was kept in a dark environment.

The third hydrogel was prepared by blending sodium alginate (A, Merck) and gelatin from porcine skin (G, Merck). Before their use, the powders were kept in ethanol for 30 min, and they underwent a cycle of UV for 1 h. Then, the powders were mixed in d-H_2O at 60 °C under magnetic stirring to reach a final concentration of 6% w/v of A and 2% w/v of G, respectively. The alginate-gelatin (AG) solution was then cooled to 25 °C before use.

Rheological characterization and extrusion tests

A rheological characterization was carried out on the VG-RGD, GGMA and AG solutions to obtain the rheological parameters to be used as an input of computational fluid dynamics (CFD) simulations. All tests were

performed using a rheometer (Anton Paar MCR-302, Graz, Austria) with a plate-plate geometry (diameter: 25 mm) on the solutions immediately after their preparation. The flow curves were acquired at 25 °C, with shear rates ranging from 0.1 to 1000 s^{-1} in rate-controlled mode by selecting 10 points for each decade. The viscosity was modeled as a Non-Newtonian fluid according to the following power law[21]:

$$\eta = K\dot{\gamma}^{n-1} \quad (1)$$

where η is the dynamic viscosity, $\dot{\gamma}$ is the fluid shear rate, K is the consistency index, and n is the flow behavior index. Then, the rheological indexes were extracted by each test (n = 4) and for each solution. The hydrogel characterization was completed with the computation of the yield stress according to the Herschel-Bulkley model[22].

We evaluated the capability of the hydrogels to flow through three different low-hardness thermoplastic biocompatible polyurethane (TPU) tubes (fixed outer diameter: 2.8 mm; inner diameters: 0.5/1.4/2.0 mm, Enki Srl), compliant to ISO 13485:2016. The test aimed to evaluate the extrusion force required to eject the materials, and to check the possible occurrence of occlusion phenomena in correspondence to the tip in the bent configuration. All the tests were performed using a Universal Testing System (model 2444, Instron, Norwood, MA, USA) equipped with a 1 kN load cell and a custom setup to hold the 5 mL syringe containing the solution and support the nitinol tip (Supplementary Fig. S1). The TPU tubes were attached to the 5 mL syringe using a needle as a connector (diameter = 15 G for 1.4- and 2.0-mm tubes, 22 G for 0.5-mm tubes, length = 10 mm, Metcal, Cypress, CA, USA). All the solutions (VG-RGD, GGMA and AG) loaded in the syringe were tested with each TPU tube by applying a controlled displacement of 5 mm at 1.6 mm/s, with both tip conditions (straight and bent), measuring the extrusion forces generated during such displacement.

Assembly of the extruder and supply units

The arthroscopic extruder comprised three main parts: a handle, a case, and a terminal part made of a cannula and a tip. Figure 2a shows the assembled handheld device; a detailed view of its components is shown in Fig. 2b: the nitinol tip and the metal cable (1), the connectors (2), the fixed cannula (3), the internal rod (4), the transmission cylinder (5), the manual trigger (6), the linear guide (7), the case (8), the handle (9), the wheel (10) and the spring (11). An eyelet on the top of the handle allowed controlling the axial rotation of the tip, through a wheel, a spring, and a bearing. The wheel was made of aluminum, the spring was a commercial steel spring,

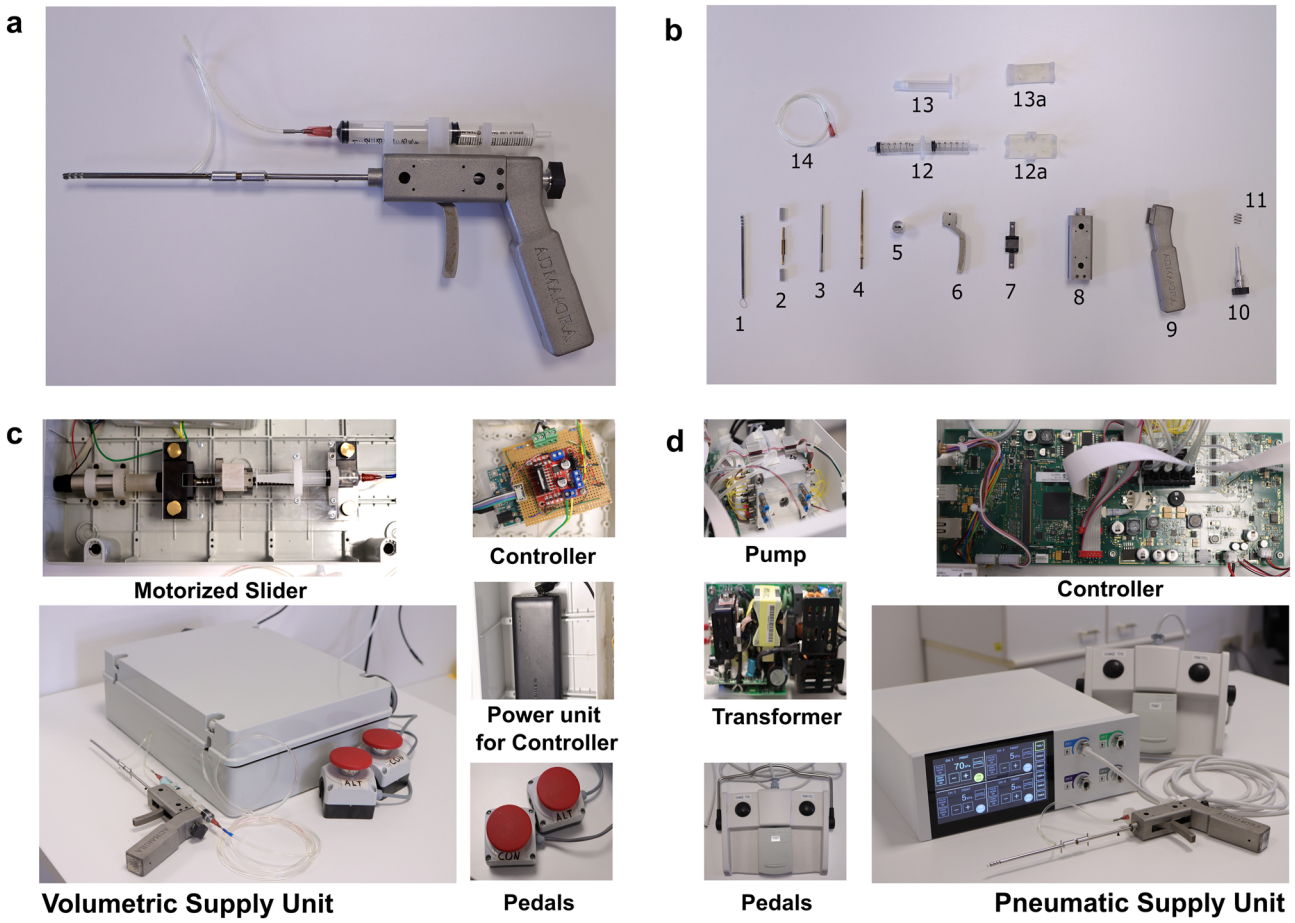

Fig. 2. Images of the handheld arthroscopic device prototype. (**a**) Assembled handheld extruder and (**b**) all its components; (**c**) main components of the volumetric supply unit and picture of the integrated system; (**d**) main components of the volumetric supply unit and picture of the integrated system.

and the bearing was made of Teflon. The rotation was controlled by pushing and rotating the wheel using the thumb. A commercial linear guide (Misumi Group Inc, Japan) was placed within the case, to which the trigger was screwed. The trigger, the case and the handle were fabricated through Selective Laser Sintering (SLS) by 3D Metal Srl (Bologna, Italy) and were held together with screws. An internal brass rod passed through a hole in the trigger, and was constrained using two Teflon bearings and two Seeger rings. In this configuration, the rod was rigid with the translational movement of the trigger, but it could rotate along its axis. A connection element made of aluminum on the terminal part of the rod was screwed to transmit the rotation from the wheel to the rod. The other extremity of the internal rod presented a perforated cap, to which the metal cable was constrained. In this way, the trigger and the cable were connected: pulling the trigger allowed the control of the tip bending. The cannula (made of aluminum) was constrained to the case using a bearing and two Seeger rings, allowing the rotation along its axis. The presence of a grain permitted the transmission of the rotational movement from the rod to the cannula. The tip and the cannula were connected by a threaded component and two bushes. In this way, the rotational movement (controlled using the wheel) was transmitted to the terminal part of the tip. Once assembled, these components allowed both the bending and the rotation of the tip, as shown in Supplementary Video S2. The tip was designed to be removed and allow the device sterilization after each surgical operation.

A commercial syringe for the volumetric system (5 mL) (12, and the corresponding holder 12a in Fig. 2b), or a commercial cartridge for the pneumatic system (3 mL, Terumo, Japan) (13, and the corresponding holder 13a) containing the hydrogel was mounted on the handle top side, and directly connected to the supply unit by the polymeric tube (14). The extruder equipped with all the components had a total weight of 355 g.

The main components of the volumetric and pneumatic supply units are shown in Fig. 2c,d, respectively. The motorized slider within the volumetric supply unit (Fig. 2c) was actuated by a DC Micromotor (Faulhaber Series 1727 CXR, Max torque: 49 mN m) equipped with a magnetic encoder (Faulhaber Series IE2-16). The motor was connected to precision ball screws through a transmission set, which moved a plunger connected hydrodynamically with the hydrogel cartridge. The system was activated by two pedals: one enabling continuous extrusion and the other one allowing a more finely controlled extrusion. The communication between the pedals and the motor was controlled through an Arduino Due microcontroller (Arduino, Italy), to set the rotation velocity and the duty cycles. The continuous extrusion allowed the surgeons to release whatever quantity of hydrogel at a determined rate, depending only on the duration of the pedal pressure. The controlled extrusion was based on a pre-set number of motor revolutions, to release always the same quantity of hydrogel after a single pedal pressure.

The pneumatic control unit (Fig. 2d) was provided by Vimex Endoscopy (Vimex Endoscopy, Gliwice, Poland). It consisted of three main blocks: (1) the first block comprised transformer components (AC filter with *medical switching mode* power supply) working in the range of 100–240 V AC for 50/60 Hz; (2) the second block included a main compression reservoir, 4 channel reservoirs, 2 pneumatic valves, electronics to drive pneumatic valves and interconnection tubing. A dedicated electronic board drove the pneumatic valves. The system also included an extra compression pump (compression up to 200 kPa) to guarantee the overpressure supply to the main compression chamber; (3) the third block comprised the main electronics board, which covered the following functions: system-on-module, pressure measurement, footswitch serving, driving the pneumatic block, I/O. A touchscreen display was implemented in the pneumatic control unit to intuitively control the extrusion parameters.

Supplementary Video S3 shows the arthroscopic extruder in action, supplied first by the volumetric unit and then by the pneumatic one.

Computational fluid dynamics simulations

CFD simulations were performed by means of COMSOL Multiphysics v6.0 (COMSOL Inc., Sweden). VG-RGD, GGMA and AG were modeled as non-Newtonian incompressible fluids. The coefficients K and n derived from the rheometric measurements were used to model the fluids according to the power law of Eq. (1). The maximum allowable plunger velocity (1.6 mm/s) according to the ISO standards (BS EN ISO 7886-1:2018) was considered for the volumetric system, while the minimum extrusion pressure for releasing the material was considered to evaluate the pneumatic system (this corresponded to 5 kPa for VG-RGD, 6 kPa for GGMA and 30 kPa for AG). Velocities equal to 0.16 and 0.016 mm/s were also considered for the volumetric extrusion. The tube having the intermediate internal diameter (1.4 mm) was included in the model determining the fluid domain, and the bent tip configuration was considered as a worst-case situation. A uniform zero-pressure was set at the system outlet, and a *no-slip* condition was imposed at the system walls. The fluid volume was meshed using a tetrahedral grid with average element size equal to 10^{-5} m. The Navier–Stokes equations for steady-state laminar flows were applied, using a convergence criterion set at 10^{-5}.

Resolution tests

For the volumetric system, the minimum number of motor revolutions to extrude the materials was evaluated by extruding each hydrogel starting from 1 revolution, and then increasing the number of revolutions until the material was released. The minimum quantity of extruded hydrogel was measured by applying three different extrusion speeds (0.016, 0.16 and 1.6 mm/s), according to the ISO standard (BS EN ISO 7886-1:2018).

For the pneumatic system, the pulse mode was set to obtain a controlled extrusion over time, using the pressure and the extrusion time as variables. These variables were empirically evaluated to understand the conditions allowing the release of the minimum volume of material.

The hydrogels were extruded on a Teflon substrate for both extrusion units, keeping the nitinol tip in both straight and bent configurations. Moreover, the end part of the tip was put either in contact with the substrate (contact configuration) or at ~ 1 cm distance from it (fall configuration). A precision balance (Entris High-Precision Balance, Sartorius) was used to weigh the amount of material extruded, in the different configurations.

Biological characterization of cell-laden hydrogels

Cell-laden hydrogels preparation and printing process

Human Chondrocytes (HCs, 402-05a, Cell Application, Inc) were thawed and cultured with their GM (Cell Application, Inc). At passage 5, cells were trypsinized and embedded within the VG-RGD, GGMA and AG solutions (density: 200,000 cells/mL) at RT. Then, the cell-laden solutions were loaded into 5 mL or 3 mL syringes, to be used in the volumetric or pneumatic systems, respectively.

An extrusion speed of 1.6 mm/s was applied to deposit all solutions for the volumetric configuration. On the other hand, a pressure of 5 kPa for VG-RGD, 6 kPa for GGMA solutions, and a pressure of 30 kPa for AG solution were set to allow hydrogel deposition with the pneumatic system. All extrusions were performed within a PDMS mold featured by a cylindrical cavity (diameter: 10 mm, height: 3 mm). This led to the delivery of slightly different hydrogel volumes (in the range 100–150 µL) depending on the extrusion conditions. Right after the extrusion, each sample was weighed with the precision balance and the weight was used to normalize metabolic activity readings, as described below. Then, each hydrogel was crosslinked following different steps. The cell-laden VG-RGD hydrogels were left stabilizing for 20 min at RT. Then, 1 mL of GM was placed over the hydrogels before incubation at 37 °C and 5% CO_2 to reach a complete ionic crosslinking. The cell-laden GGMA hydrogels were photo-crosslinked upon deposition by a cold LED source (RfQ—Medizintechnik-GmbH & Co), setting a distance of 1.5 cm and a light intensity of 18 mW cm^{-2} for 60 s. Then, 1 mL of GM was placed over the hydrogels before incubation at 37 °C and 5% CO_2. The cell-laden AG hydrogels were ionically crosslinked by pouring 1 mL of calcium chloride ($CaCl_2$, 1% w/v, Merck) on top of them, and waiting for 10 min. Then, the ionic solution was removed, and 1 mL of GM was placed over the hydrogels before incubation at 37 °C and 5% CO_2. The culture medium was renewed daily.

Live and dead assay

The viability of HCs embedded into VG-RGD, GGMA and AG hydrogels was evaluated after 1, 3 and 7 days through the Live/Dead assay (Life Technologies, ThermoFisher Scientific, USA). According to the manufacturer's instructions, the samples were washed thrice in PBS for 5 min at 37 °C and then incubated with the Live/Dead solution for 45 min at 37 °C. After staining, hydrogels were washed three times for 5 min at 37 °C with PBS, then evaluated with a confocal fluorescence microscope (Nikon Instruments Europe BW). Living cells were observed in green, while dead cells were identified in red. Different planes at a distance of 200 µm were acquired all along the section of the hydrogel.

Metabolic activity assay

Cell metabolic activity was analyzed on day 1, 3 and 7 using the PrestoBlue assay (Invitrogen, ThermoFisher Scientific, USA). According to the manufacturer's instructions, the samples were washed with PBS for 5 min at 37 °C and then incubated with the PrestoBlue solution diluted in HC Growth Medium (ratio 1:10) for 1 h. Then, the supernatants were collected, and the absorbance was read at 570 nm using an automated spectrophotometric plate reader (Victor Nivo, Perkin Elmer, USA). Data were normalized, for each sample, with respect to the sample weight.

Usability test on human cadavers

An ex vivo test was performed on a male knee available at a dedicated teaching and research surgical center (Multimedica Srl, Milano, Italy), fully accredited for cadaver management. All methods were carried out in accordance with relevant guidelines and regulations. The experimental protocols did not require the approval by any University ethics committee. In fact, tests on human cadavers were carried out taking care of the following principles: respect for persons, beneficence and justice, exploiting a fully accredited structure for this kind of tests, namely Multimedica Srl, Milano, Italy. This structure provided all the equipment and organizational support in order to perform the tests, which guaranteed all ethical-legal aspects. The Cadaver Lab guaranteed indeed that the anatomical preparations came from the United States (provided by Science Care, USA) and belonged to donors who had personally expressed their informed consent to the donation; all donors (and their families) in fact, have completed a donation authorization consent form. They were corpses serologically tested at the origin and not belonging to unclaimed remains. The specialized structure also ensured the security and safety of the workplace for surgeons and researchers who will perform the test. All procedures were performed in a fully-equipped surgical room, with proper individual protection devices and clothes. The left knee used for the test belonged to a person with the following features: age: 48; gender: male. Nine orthopedic surgeons were involved: all of them were asked to release a proper quantity of hydrogel upon four cartilage defects (average diameter ~ 7 mm) specifically created in different points of the cadaver knee cartilage. Informed consent was obtained from all subjects involved. To prevent any possible bias in the final feedback, the surgeons were divided into two groups: the former (5 surgeons) started the test using the extruder with the volumetric supply unit; the latter started using the extruder with the pneumatic supply unit. Then the groups switched the instruments and continued testing them. For the volumetric system, an input velocity equal to 1.6 mm/s was imposed; for the pneumatic system, a pressure of 30 kPa was used as the input. The AG was used in this test; it was mixed to a blue dye (Blue, Davidson Marking System) to make it more visible during the procedure.

Statistical analyses

A normality test (D'Agostino-Pearson) was performed on all experimental data to assess data distribution. In all cases, data resulted having a non-normal distribution. For statistical comparisons, a non-parametric Kruskal–Wallis' test and Dunn's multiple comparison test were applied, to analyze significant differences between

the groups. Statistical analyses were carried out using GraphPad Prism (v 8.0.2). The significance threshold was set at 5%.

Results

Design and mechanical characterization of the tip

The nitinol tip dimensioning was set in collaboration with expert clinicians from the Istituto Ortopedico Rizzoli, who are co-authors of this work. The tip length was set to 92 mm, a value that allowed reaching the most internal areas of the knee; the outer diameter was set to 4 mm. The wall thickness was set to 0.25 mm, guaranteeing an internal diameter equal to 3.5 mm. The distal part of the tip was composed of three modules, each able to bend up to 30°, made of a flap and a notch (Fig. 3a). Such a design allowed to bend the tip in one direction up to 90°, reaching an orthogonal position between the tip's main axis and the cartilage defect to be treated. The module dimensions were chosen to maintain the axial encumbrance as small as possible (7 mm), coherently with other arthroscopic tools having a bent extremity, like probes, forceps and rasps[23]. The bending of the tip was possible by pulling the metal cable: this element passed internally between the nitinol tip and the polymeric tube and it was constrained to the last module of the tip and the trigger, respectively, at the two extremities (Fig. 3a).

Four possible tip designs were investigated, with the aim of identifying the optimal one in terms of stress concentration, bending force, resistance to bending in undesired directions, and fatigue resistance. These features were analyzed through Finite Elements (FE) simulations and experimental measurements. The four tip versions are sketched in Fig. 3b: Version A was featured only by the notches allowing the bending, while the other versions included additional details inspired by the state-of-the-art[24–26]. In particular, Version B included incisions on the back side of the tip, Version C included abutments to smooth the angles of each module (and to avoid overlapping), while Version D included both incisions and abutments.

An initial assessment was performed through FE simulations, regarding von Mises' stress distribution and bending force in correspondence to a 90° bending. Figure 3c shows similar distributions of von Mises' stresses among all versions (735 MPa was the maximum stress value found for Version A, 715 MPa for Version B, 704 MPa for Version C and 680 MPa for Version D). However, it can be observed that the versions provided with the abutments helped the flaps to discharge the stress. The stress was equally distributed among the three

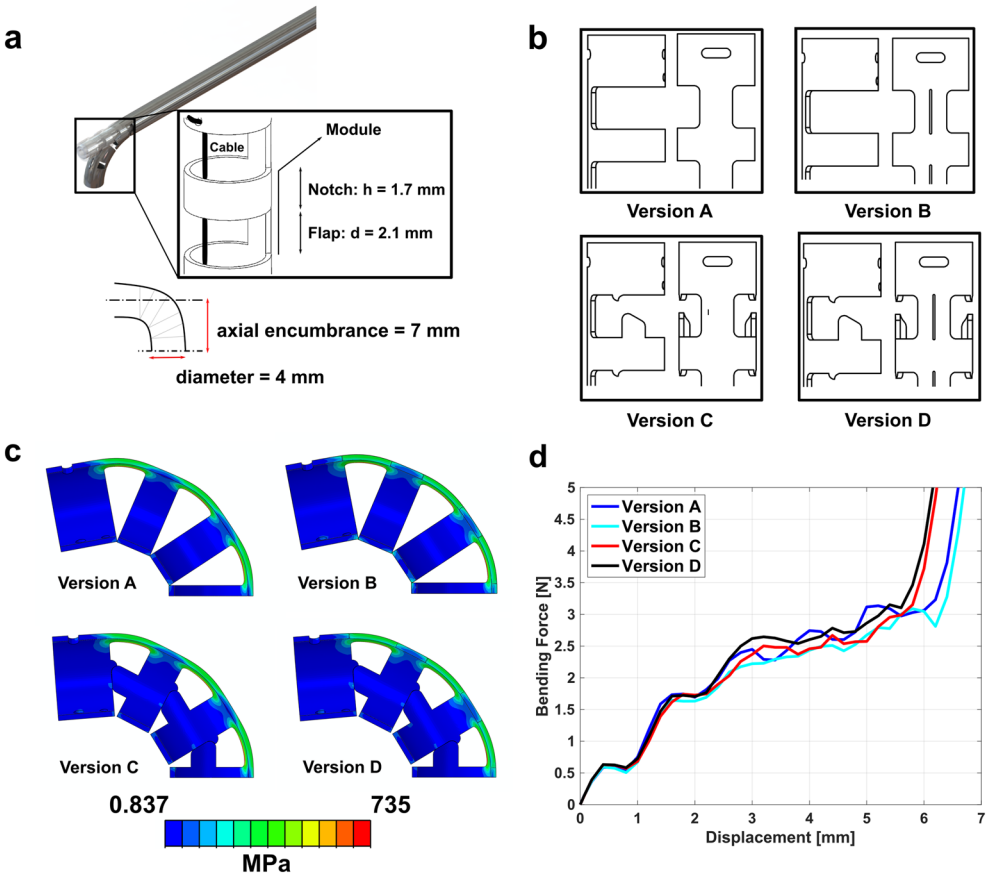

Fig. 3. Nitinol tip design. (**a**) Dimensions and geometrical features common to all tip versions; (**b**) depiction of the four tip versions considered in the design phase; (**c**) results of the FE analysis imposing a 90° bending to the tips and assessing von Mises' stress distribution; (**d**) results of the FE analysis in terms of estimated force needed to bend the tip.

modules in all tip versions, while the highest values were limited to the flap sides. The tip bending was simulated by applying a vertical displacement to a virtual cable constrained to the last notch (not visible for the sake of clarity). The force needed to bend the tip, for each version, is shown in Fig. 3d. The trends and the values of the estimated forces were similar for all versions: they differed from less than 0.6 N (Version A: 3.2 N, Version B: 2.7 N, Version C: 2.6 N, Version D: 2.9 N, at 5 mm).

FE simulations did not highlight any relevant differences among the four versions. Experimental tests were thus carried out to better discriminate the mechanical behavior of the nitinol tips. The aim was to find a trade-off between the possibility to bend the tip with ease, and its resistance to repeated stresses.

The experiments were performed using a traction test machine. First, the force needed to bend the tip up to + 90° was assessed using the setup depicted in Fig. 4a. The cable, tied to the tip, was pulled by the machine while the values of force were read by the load cell. The results of this test are reported in Fig. 4b. The curves of the four tip versions resulted overlapped with similar values, and reaching a maximum force of ~ 4.5 N at a displacement of 6.7 mm, corresponding to a bending angle of + 90°. These force values guarantee the surgeon to bend the tip multiple times during the procedure without excessive effort. The measured force values closely matched those estimated by the FE simulations (Fig. 3d), which can be considered properly validated.

The same setup (Fig. 4a) was used to explore the correlation among the bending force, the bending angle and the displacement of the cable for all the tip versions. The outcomes of this test are shown in Supplementary Fig. S2, highlighting a similar behavior between all versions. A movie of the tip bending up to + 90° is shown in Supplementary Video S1.

In the in vivo scenario, the tip is expected to encounter and touch various obstacles before reaching the desired area. Therefore, a second test was performed to investigate the behavior of the tip when it was bent in undesired directions. For this purpose, a 3D-printed component was pressed down with the test machine, bending the tip up to − 90° (Fig. 4c) and then leaving it free and evaluating how efficiently it recovered the original shape. We found that the incisions on the back of the tip resulted in a more uniform stress distribution and avoided excessive local stresses. Therefore, Versions B and D showed better elastic recovery than Versions A and C when the weight was removed (Fig. 4d). Finally, between Version B and Version D, the tip with the abutments (Version D) was chosen. Indeed, this feature allowed the tip to stop its bending more accurately at + 90° without an

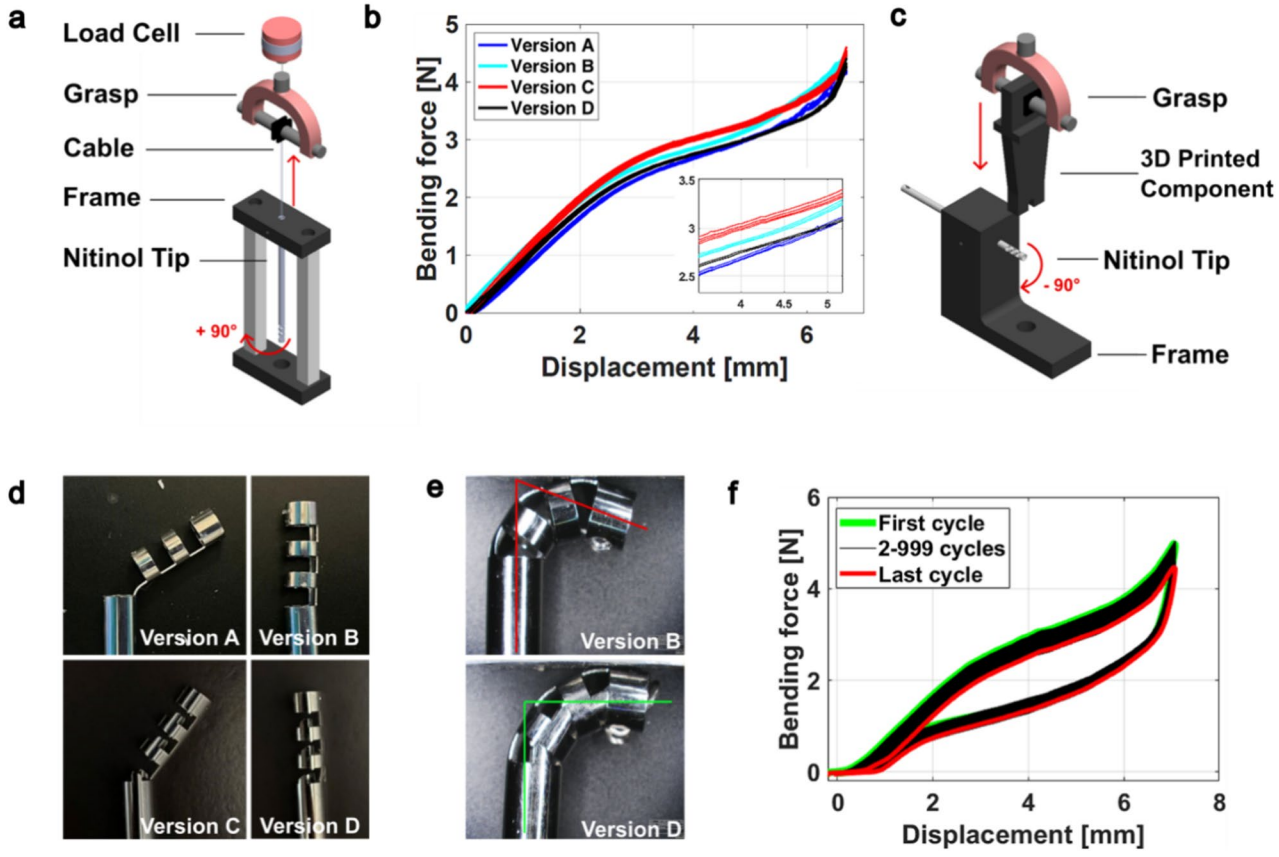

Fig. 4. Mechanical characterization of the four tip versions. (**a**) Setup for measuring the force needed to bend the tip; (**b**) tip bending force measured against the grasp displacement; (**c**) setup for the characterization of the tip behavior when bent in an undesired direction (− 90°); (**d**) images of the four tip versions after bending the tip in the undesired direction and after removing the weight; (**e**) comparison between Version B and Version D of the tip in terms of precision in reaching a + 90° bending angle; (**f**) fatigue analysis (1000 bending cycles) performed on tip Version D.

overlap of its modules, as shown in Fig. 4e. This feature also allowed to limit the overbending of the modules, which could cause the tip to break inside the knee. As a result of these quantitative and qualitative tests, Version D was selected as the final tip design. Then, its long-term durability was investigated by a fatigue analysis, using the setup presented in Fig. 4a. Figure 4f shows that the force required to bend the tip after 1000 cycles is slightly smaller than the original one. Thanks to the *superelastic* properties of nitinol, no plastic deformation occurred.

Rheological characterization and extrusion tests

Three different hydrogel types were tested to verify their usability with the proposed handheld extrusion device. VG-RGD at a concentration of 1:2 has been recently proposed as an optimal hydrogel supporting the chondrogenesis of adipose-derived stem cells[19]. GGMA is a methacrylated version of gellan gum, which has been recognized as a promising material for cartilage tissue engineering, due to its structural similarity with glycosaminoglycans[20,27]. Lastly, a blend of alginate and gelatin (AG) has been recently proposed in the cartilage tissue engineering field[28]. This material was selected also to verify the behavior of the proposed extrusion system when using relatively viscous hydrogels.

A rheological characterization of the different hydrogel types (VG-RGD, GGMA and AG) was performed. As reported in Fig. 5a, the viscosity *vs.* shear rate curves found for VG-RGD and GGMA were similar, whereas the viscosity of AG decreased less rapidly when the shear rate increased. Rheological indexes typical of non-Newtonian fluids (K and n) were extracted by the flow curves of the different materials. They are reported in Table 1. The AG solution showed the highest consistency (K, average value: 3.89 ± 1.05 Pa s^n) and flow behavior indexes (n, average value: 0.63 ± 0.07), while no significant differences were found between VG-RGD and GGMA. The yield stress of the hydrogels was estimated by applying the Herschel-Bulkley model. GGMA was featured by the highest yield stress values (τ_0: 0.91 ± 0.24 Pa), in comparison to VG-RGD and AG. However, the data were not statistically different.

The extrusion characterization was carried out following ISO 13485:2016. The extrusion forces required to flow out the three hydrogels through three different TPU tubes were measured, with a displacement rate of 1.6 mm/s, for the volumetric system. TPU tubes were featured by internal diameters of 0.5, 1.4, and 2 mm, respectively. The tip configuration was also varied (straight tip or 90°-bent tip). The setup used to perform this test is shown in Supplementary Fig. S1. Figure 4b shows the extrusion forces recorded using a tube with a diameter of

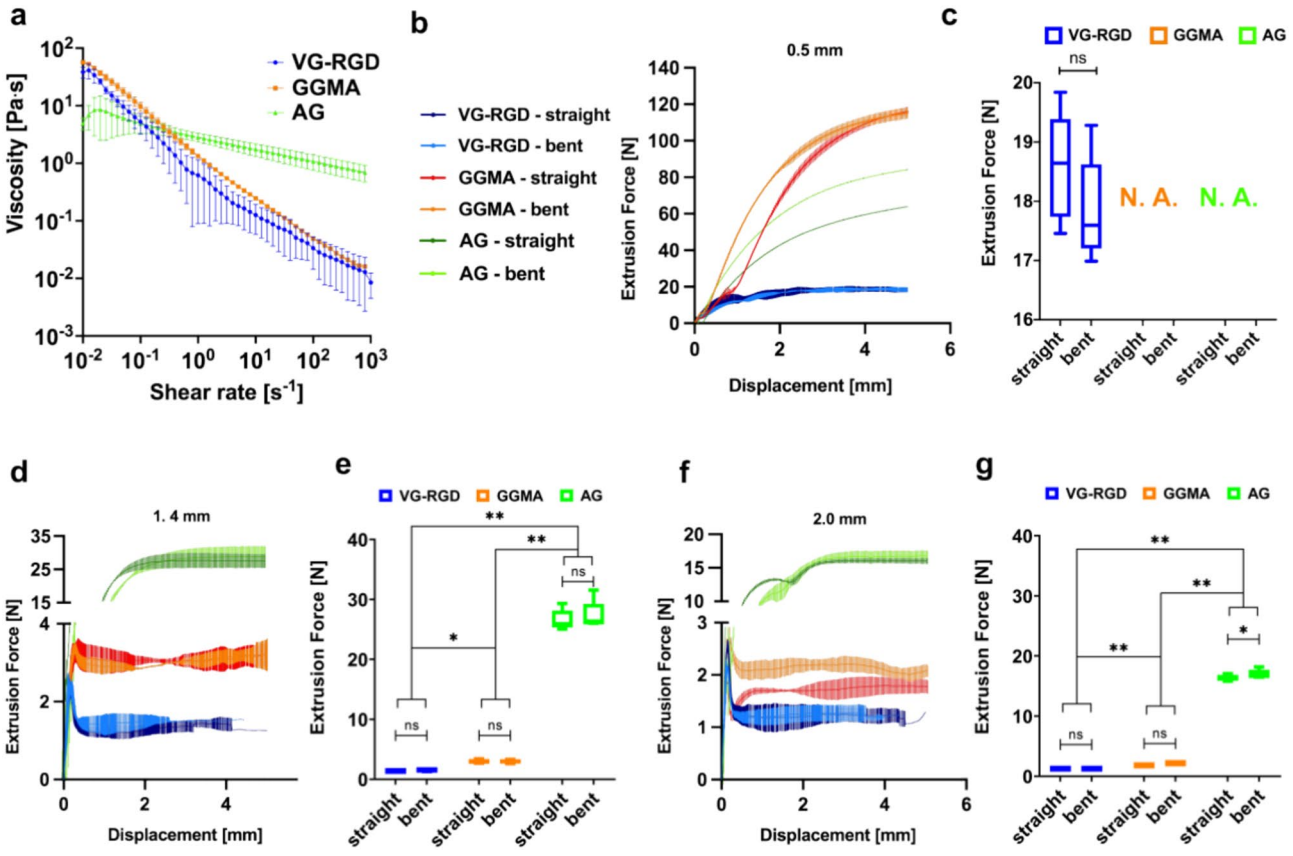

Fig. 5. Rheological characterization and extrusion tests for the hydrogels used in this study to validate the handheld device. (**a**) Viscosity *vs.* shear rate curves of VG-RGD (blue), GGMA (orange) and AG (green); (**b**, **d**, **f**) extrusion force vs. plunger displacement for the different hydrogels, pushed through polymeric tubes having a diameter of 0.5, 1.4 and, 2.0 mm. (**c**, **e**, **g**) Comparison of extrusion forces obtained with both straight and bent tip configurations, and between the three hydrogel types; $^*p < 0.05$; $^{**}p < 0.01$.

	VG-RGD	GGMA	AG
K [Pa s^n]	1.12 ± 0.36	1.71 ± 0.12	3.89 ± 1.05 (*) (#)
n	0.30 ± 0.04	0.26 ± 0.01	0.63 ± 0.07 (*) (#)
τ_0 [Pa]	0.56 ± 0.29	0.91 ± 0.24	0.46 ± 0.33

Table 1. Rheological indexes (K, n) and yield stress (τ0) extracted from VG-RGD, GGMA, and AG flow curves. Data are reported as mean ± SD, n = 4; *p < 0.05: it is referred to the comparison between VG-RGD and AG. #p < 0.05: it is referred to the comparison between GGMA and AG.

0.5 mm. Here, a plateau was reached only for VG-RGD extrusion, with both straight and bent tip configurations. Differently, the extrusion forces needed for GGMA and AG increased without reaching a plateau, meaning that such hydrogels were challenging to extrude using a tube with that diameter. The impossibility of achieving a plateau meant that a finely controllable extrusion was not possible. In the case of the VG-RGD, no statistically significant differences were found between the plateau values achieved with the straight (18.58 ± 0.91 N) and the bent (17.85 ± 0.87 N) tip configurations (Fig. 5c).

In the case of the 1.4 mm diameter, the extrusion forces curves reached a plateau for all materials, with both straight and bent tip configurations (Fig. 5d). The force needed to extrude the VG-RGD was (1.39 ± 0.13 N) and (1.54 ± 0.16 N) for straight and bent configurations, respectively. Similar values were found for the GGMA, which reached 2.99 ± 0.26 N with a straight tip, and 2.99 ± 0.26 N with a bent tip configuration. AG showed extrusion higher forces equal to 26.57 ± 1.68 N and 27.35 ± 2.38 N, for straight and bent configurations, respectively. In this case, no statistically significant differences between the tip configurations were found for any hydrogel type (Fig. 5e).

Also in the case of the 2 mm diameter tube, the extrusion forces reached a plateau (Fig. 5f). The force values were 1.26 ± 0.12 N (straight) and 1.25 ± 0.13 N (bent) for VG-RGD, 1.8 ± 0.12 N (straight) and 2.15 ± 0.09 N (bent) for GGMA, and 16.36 ± 0.51 N (straight) and 17 ± 0.72 N (bent) for AG, respectively. No statistically significant differences were found between straight and bent tip configurations during the extrusion of VG-RGD and GGMA, while a significant difference was found for the extrusion of AG, between the two tip configurations (Fig. 5g).

Computational fluid dynamics simulations

Computational fluid dynamics (CFD) simulations were performed through COMSOL Multiphysics v6.0 using as an input the rheometric parameters reported in Table 1 for the different materials. The simulations aimed at evaluating the presence of localized peaks of wall shear stress (WSS) during the extrusion of VG-RGD, GGMA and AG, as these could compromise the viability of the cells embedded in the hydrogels. To this aim, the extrusion conditions for both supply units were simulated. In particular, the maximum allowable plunger velocity (1.6 mm/s) according to the ISO standards (BS EN ISO 7886-1:2018) was taken into account for the volumetric extrusion, together with smaller velocities (0.16 and 0.016 mm/s), while the minimum extrusion pressures (obtained during resolution tests, shown in the next section) were considered to evaluate the pneumatic extrusion (5 kPa for VG-RGD, 6 kPa for GGMA, and 30 kPa for AG). The intermediate tube diameter (1.4 mm) was selected, and the bent tip configuration was considered as a worst-case situation.

The simulations were firstly compared to the extrusion characterization test in terms of extrusion forces, as shown in Fig. 6a. The agreement between the CFD results and the experimental measurements (max error ~ 5%—AG with 1.6 mm/s inlet velocity) served as validation. The higher error in AG was probably due to the higher friction effects due to this material, which were not considered in the simulations.

The different material rheometric properties influenced the shear stress estimation, as shown in Fig. 6b. The maximum values of materials' wall shear stress (WSS) obtained for AG extruded at 1.6 mm/s with a bent tip (up to 416 Pa) were more than ten times higher than the ones found for the other materials and extrusion conditions. The inlet velocity also slightly affected the WSS in the case of volumetric extrusion: a 100 times higher inlet velocity led to 4 times higher WSS values. The water-like properties of VG-RGD and GGMA led to lower stress values, up to 32 Pa for the GGMA and up to 17.6 Pa for the VG-RGD. A similar behavior was found considering the minimum extrusion pressure for the pneumatic unit.

Resolution tests

The performance of the device supplied by the volumetric unit and by the pneumatic unit, was evaluated in terms of resolution, namely the minimum quantity of material that could be released by the device. As the treatment of cartilage defects can regard areas of different dimensions, occasionally involving small focalized points, the device volume resolution is an important parameter for evaluating its possible use in a real scenario. The resolution was evaluated under different conditions: with the tip straight or bent, and with the position of the tip with respect to the surface was in direct contact (contact) or at a ~ 1 cm distance (fall), as shown in Supplementary Fig. S3. The quantity of material extruded on a Teflon cylinder was measured with a precision balance, in the different conditions.

Concerning the volumetric unit, the resolution was related to the minimum number of motor revolutions allowing material extrusion. This was set experimentally. They resulted in 4 motor revolutions for VG-RGD and GGMA, and 15 for AG in the contact condition. In the fall condition, they resulted in 7 motor revolutions for VG-RGD, 9 for GGMA, and 20 for AG. For each configuration, three different extrusion speeds (0.016, 0.16,

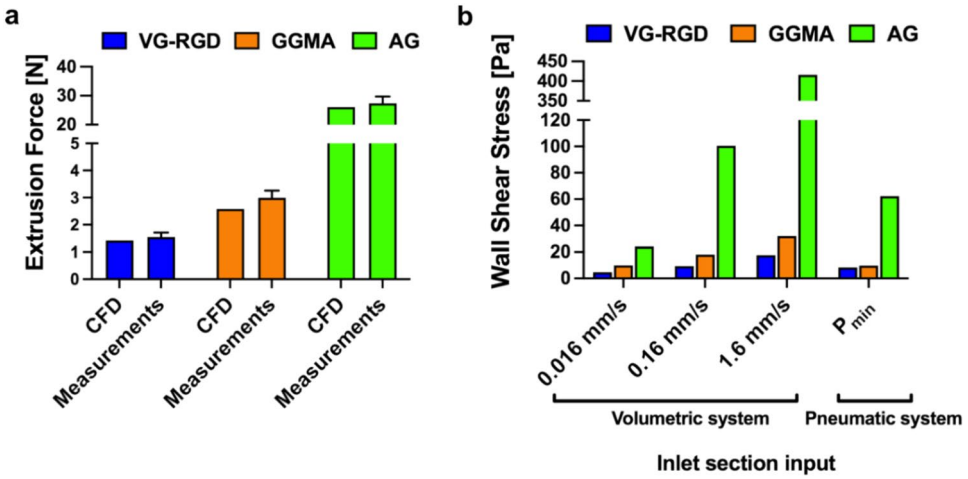

Fig. 6. CFD simulation results. (**a**) Comparison between the extrusion forces obtained via CFD simulations and experimental measurements; (**b**) estimation of the wall shear stress obtained for the different materials extruded through the 1.4 mm polymeric tube with a bent tip, taking into account both volumetric (with different velocities) and pneumatic supply units.

1.6 mm/s) were considered. The results collected for the VG-RGD and the GGMA are shown in Fig. 7a,b, respectively. The extrusion of GGMA in different conditions is also shown in Supplementary Video S4. With the tip straight and in contact condition, the average quantity of VG-RGD released was 21.6 µL, while for the GGMA it was 23.6 µL (input velocity: 1.6 mm/s). These quantities matched with the ones expected (24 µL), calculated considering the known plunger displacement due to the motorized slider actuation. Differences between contact and fall conditions were evident (36.6 µL for VG-RGD, 46.6 µL for GGMA), while no differences were observed between the straight and the bent tip configurations. As it concerns the AG, the minimum extrusion speed of 0.016 mm/s was not considered, as the extrusion time resulted higher than 60 s (due to a higher number of motor revolutions needed to extrude the material). This time was considered too long for a smooth clinical use. Accordingly, the resolution was tested only by imposing 0.16 and 1.6 mm/s (Fig. 7c). The AG extrusion had a smaller resolution, with an average released quantity of 71 µL (straight tip in contact position, 1.6 mm/s). For all materials, the resolution was not influenced by the imposed velocity.

The resolution of the pneumatic extrusion unit was linked to the minimum extrusion pressure and the minimum extrusion time for which the material could be extruded. These values were identified after experimental attempts. VG-RGD was supplied by setting a pressure of 5 kPa for 600 ms in contact condition and 980 ms in fall condition; the quantities extruded are plotted in Fig. 7d. GGMA was extruded with a pressure of 6 kPa for 600 ms in contact, and 980 ms in fall condition (extruded quantities in Fig. 7e). Finally, AG was extruded with a pressure of 30 kPa applied for 500 ms in contact, and 760 ms in fall condition (extruded quantities in Fig. 7f).

It can be observed that the pneumatic extrusion led to a better resolution compared to the volumetric one. Indeed, the extruded quantity was reduced up to 70% (in the contact configuration). With this supply unit, the differences between the materials were less evident: the minimum quantity of AG released (15 µL) was slightly larger than the one of VG-RGD (5 µL) and GGMA (6.3 µL), with the straight tip in contact condition. Significant differences were observed between the contact and fall conditions, similarly to the volumetric approach.

Biological characterization of cell-laden hydrogels

Biological analyses on cell-laden hydrogels were performed to assess how cell viability and metabolic activity were influenced by the extrusion process. Tests were performed by extruding ~ 150 µL of material containing HCs into a mold, keeping the device tip in the bent configuration and in the contact modality. The material was subsequently crosslinked as described in the section "Resolution tests". An extrusion speed of 1.6 mm/s was set to deliver all materials with the volumetric configuration, while a pressure of 5 kPa, 6 kPa and 30 kPa was set to extrude VG-RGD, GGMA and AG, respectively, with the pneumatic configuration.

As shown in Fig. 8a,b, HCs embedded into the three hydrogels resulted alive after 1, 3, and 7 days from the extrusion, with both supply units. Cell shape was more elongated within the VG-RGD hydrogels with respect to the other materials (GGMA and AG). However, comparing the materials extruded with the volumetric and pneumatic systems, no significant differences were qualitatively found in the cell shape and distribution. Materials also differed in terms of cell metabolic activity. The HCs embedded into VG-RGD hydrogels increased the metabolic activity markedly from day 1 to day 7 (Fig. 8c), whereas the ones embedded in GGMA showed a less evident increase (Fig. 8d), and the ones embedded in AG remained constant over time (Fig. 8e). No differences were found between the volumetric and the pneumatic systems, at any time point and for each hydrogel. Consequently, the different cell behavior was mainly due to the hydrogel properties rather than the supply unit adopted. Such biological outcomes confirmed that the proposed extrusion device can be considered safe for delivering cell-laden hydrogels.

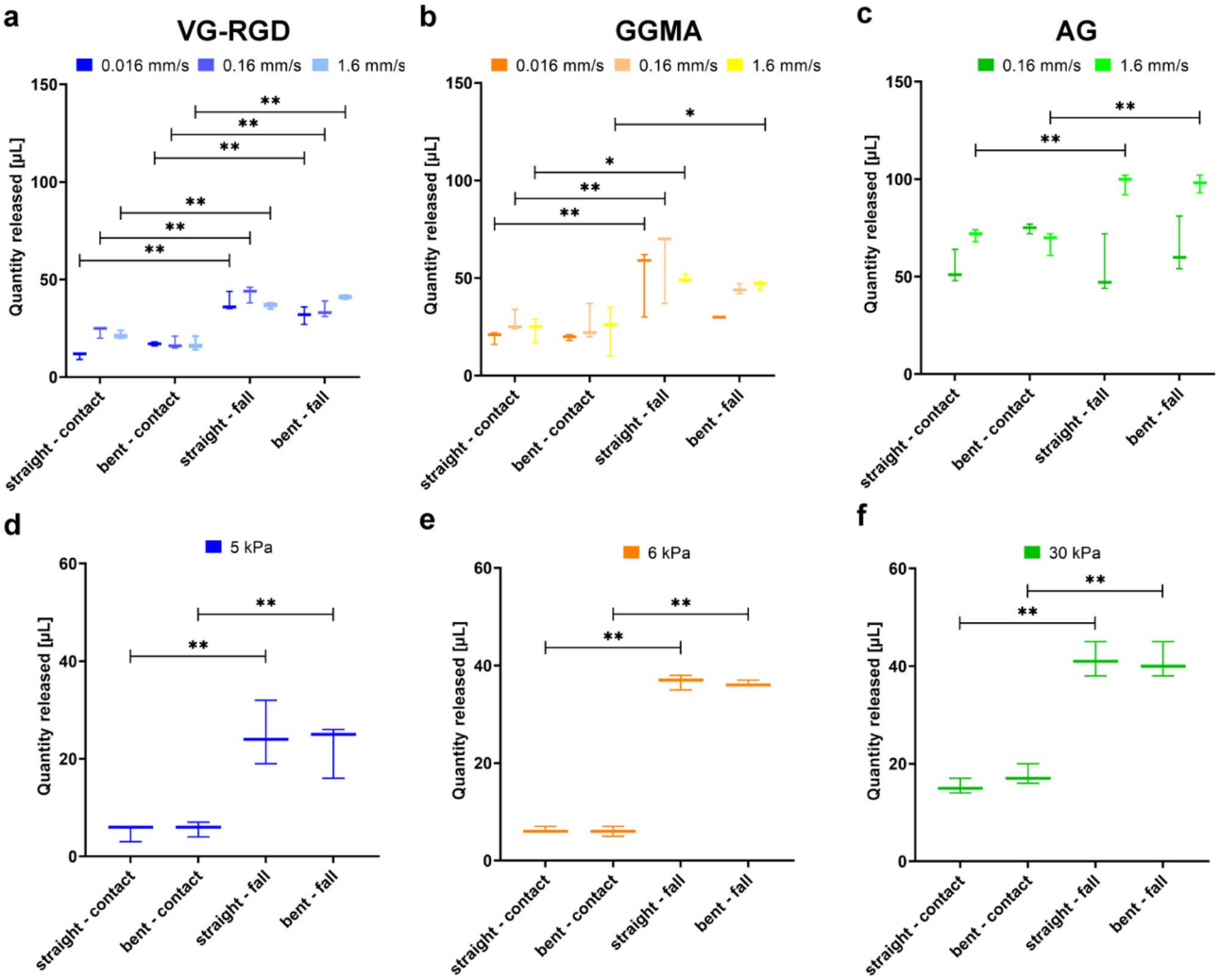

Fig. 7. Outcomes of the resolution tests. (**a**–**c**) Minimum released quantity of VG-RGD (**a**), GGMA (**b**) and AG (**c**) for different velocities imposed using the volumetric supply unit, for different tip configurations (straight and bent) and conditions (contact and fall). (**d**–**f**) Minimum released quantity of VG-RGD (**d**), GGMA (**e**) and AG (**f**) by using the pneumatic supply unit set at the minimum extrusion pressures and minimum extrusion times, for different tip configurations (straight and bent) and conditions (contact and fall); $^{*}p < 0.05$; $^{**}p < 0.01$.

Usability test on human cadavers

To validate the device in an arthroscopic setting, a usability test was performed on a human cadaver knee (Fig. 9a). Nine orthopedic surgeons tested the device by simulating an arthroscopic surgery procedure to treat cartilage lesions. Their feedback was collected through a questionnaire to identify the advantages and disadvantages of the two different extruder versions. First, four defects were created through a rasp on the cadaver cartilage tissues (Supplementary Fig. S4a), on the medial condyle (1), lateral condyle (2), medial tibial plate (3), and lateral tibial plate (4), as depicted in Fig. 9b. Each surgeon tested the extruder with both supply units (volumetric and pneumatic) delivering AG into all defects. The AG was colored with a blue dye to emphasize its visibility with the arthroscopic camera. Figure 9c shows representative images of material extrusion in the four cartilage defects.

The bendable tip allowed the surgeons to get to areas of the articular cartilage hard to reach through traditional arthroscopic tools and to deliver materials in those points (as in defects 2 and 4, Fig. 9c,d). Highlights of the test are summarized in Supplementary Video S5, which shows arthroscopic videos of AG extrusion with the volumetric and pneumatic units. After completing the usability test, the knee cartilage tissues were fully exposed to verify the in situ retention of AG on the defects (Supplementary Fig. S4b).

The surgeons evaluated the usability and performance of the two device versions (one provided with the pneumatic supply unit, the other provided with the volumetric supply unit), by filling a questionnaire after completing the test. The questionnaire was composed of demographic information, comfort-related aspects, and technical questions, with a final section in which each surgeon could give his general opinion on the device and suggestions for future improvements. The open-ended comments provided are shown in Table S1. The age of the surgeons (all male) ranged from 31 to 47 years, whereas the years of experience in the arthroscopic surgery field ranged from 1 to 15.

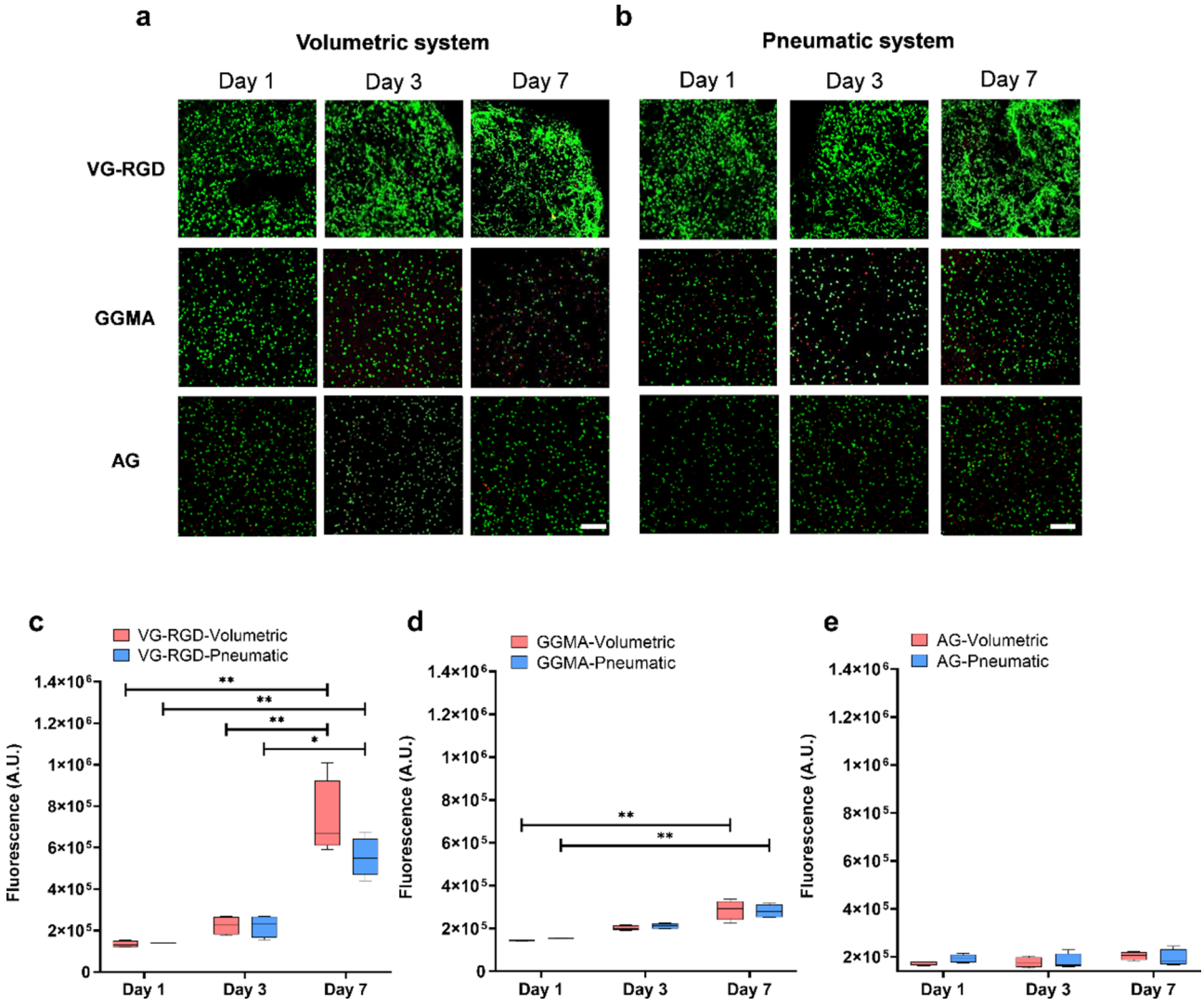

Fig. 8. Biological characterization of human chondrocyte-laden hydrogels after extrusion with volumetric and pneumatic supply units. (**a**,**b**) Live/dead assay performed on chondrocytes encapsulated in VG-RGD, GGMA, and AG hydrogels extruded with the volumetric (**a**) and the pneumatic supply unit (**b**) evaluated on day 1, day 3 and day 7; viable cells are shown in green, dead cells are shown in red. Scale bars = 250 µm. (**c**–**e**) Metabolic activity of chondrocytes embedded into VG-RGD (**c**), GGMA (**d**) and AG (**e**) after extrusion with both supply units. $^{*}p < 0.05$, $^{**}p < 0.01$.

Results (Fig. 10) showed that the shape of the handle allowed a relatively comfortable use of the extruder, with an average score 3.77 out of 5 for question B.1. No pain and low discomfort were reported in B.2, with an average score of 4.44 out of 5, although the mechanism for driving the tip in the ergonomic design could be improved (average score of 3.22 out of 5 for question B.3). Technical questions about the characteristics of the handheld extruder showed similar results between the volumetric and pneumatic systems (C.3–C.8), since the supply units were not involved in these questions. The questions regarding the tip maneuverability (C.3) and bendability (C.4) showed valuable results (average scores 4.11 and 3.66 out of 5, respectively). The tip allowed surgeons to easily reach all cartilage defects, and the most relevant scores were obtained for the defects in the medial condyle (C.5), in the medial tibial plate (C.7), and in the lateral tibial plate (C.8), which reported average scores of 4.66, 4.83, and 4.60 out of 5, respectively. A lower score was obtained for the defect in the lateral condyle (C.6): 4.22 out of 5. The most relevant differences between the volumetric and the pneumatic supply units emerged from questions C.1, C.2 and C.9. In these questions, the pneumatic system scored better in terms of ease of use (C.1) and intuitiveness of the user interface (C.2), with average scores of 4.44 and 4.37 out of 5 (against 4.11 and 3.75 of the volumetric system). Also regarding the material extrusion accuracy (C.9) the pneumatic supply unit scored better than the volumetric one, with an average score of 4.05 against 2.33. Finally, the average scores of the section focusing on the overall device evaluation, ranged from 3.44 (D.1, volumetric) to 4.22 (D.1, pneumatic–D.2, volumetric), indicating a general appreciation of the device, although the extruder equipped with the pneumatic supply unit had more desirable features.

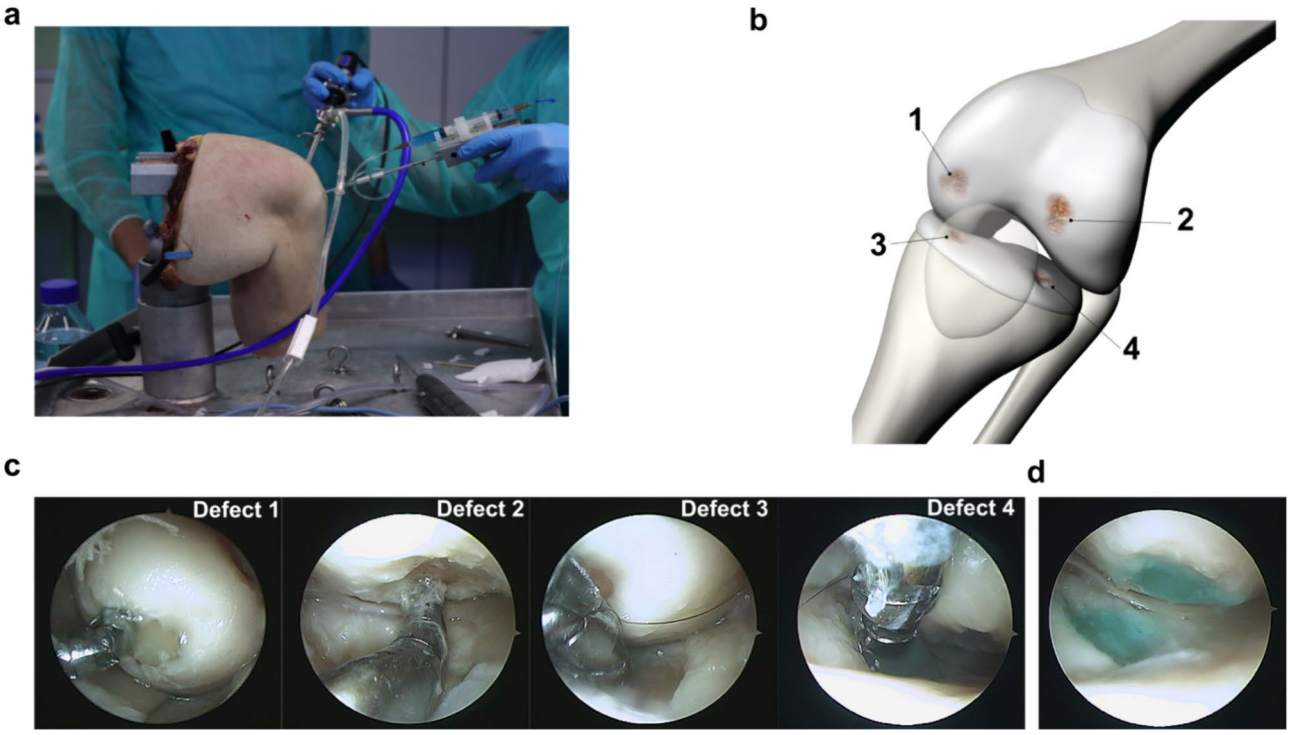

Fig. 9. Usability test on a human cadaver. (**a**) Image of a surgeon using the arthroscopic extruder on the human cadaver knee; (**b**) cartilage areas on which the defects were created. (**c**) Representative images of arthroscopic procedures aimed at extruding the material through the bendable tip on the four defects. (**d**) Representative image of defects 2 and 4 filled with the blue-colored AG.

Discussion

This work proposes a novel approach for the in situ cartilage repair of defects using a bendable arthroscopic extruder supplied by a volumetric or pneumatic supply unit.

As interest arose in portable bioprinters for tissue regeneration in the last decade, many solutions have already been presented and commercialized[29]. Their portability, the ease with which sterile material cartridges may be replaced, and the high-resolution material release in a clinical setting are the main advantages of such novel designs[13,14,30]. However, all the solutions proposed so far regarded applications for external tissues such as the skin, or required an open surgery approach, with a significant risk of infections and post-operative side effects[31,32]. The arthroscopic device proposed in this work represents a novel approach compared with these efforts. This instrument, in fact, would allow surgeons to extrude materials onto cartilage defects adopting a minimally invasive (arthroscopic) approach. The controllability of the nitinol tip confers to the device a good maneuverability and enables reaching even rather hidden areas of the articular joint, which are difficult to access with conventional instruments. Arthroscopic tools are usually straight and metallic with sharp edges, sometimes equipped with tips featured by fixed angles (such as some forceps and grasps). The use of a manually maneuverable device may reduce the risk of accidental tissue damage and increase the effectiveness of clinical outcomes[33]. Steerable surgical tools have been recently proposed for catheter-based or endoscopy-based procedures[24]. However, to the best of our knowledge, there are no similar approaches for the in situ delivery of hydrogels for cartilage-related applications.

Nitinol has been considered a candidate material for designing the tip, being broadly approved for the fabrication of medical devices, and for its *superelastic* properties, long-term resistance and biocompatibility[34]. In this work, the mechanical characterization of the nitinol tip confirmed the reliable elastic return and long-term stability (Fig. 4), although in the original shape exploited in this work. An optimal trade-off between strength and flexibility of the tip has been identified in a specific version of the tip design, featured by incisions in the back side and abutments. This finding could be of inspiration for future possible medical tools, targeting different applications but having similar requirements.

When considering a potential application of material delivery systems in humans, their sterility must be ensured. A recent example was proposed by Albanna et al.[10] for the skin bioprinting system. In this case, the device was developed with a detachable print head that can be autoclaved. In our work, the nitinol tip can be easily removed after the surgical procedure to be sterilized (e.g., with ethylene oxide) or to be replaced in case of breakage.

The rheological characterization performed on VG-RGD, GGMA, and AG through the flow curve tests showed that viscosity decreased with increasing the shear rate. In particular, VG-RGD and GGMA showed a similar viscosity trend, whereas the AG showed a higher viscosity at higher shear rates (after 1 s^{-1}). However, all hydrogels demonstrated a shear-thinning behavior, suggesting their use as injectable materials and that the assumption of non-Newtonian fluids modeled with the power law was acceptable[35].

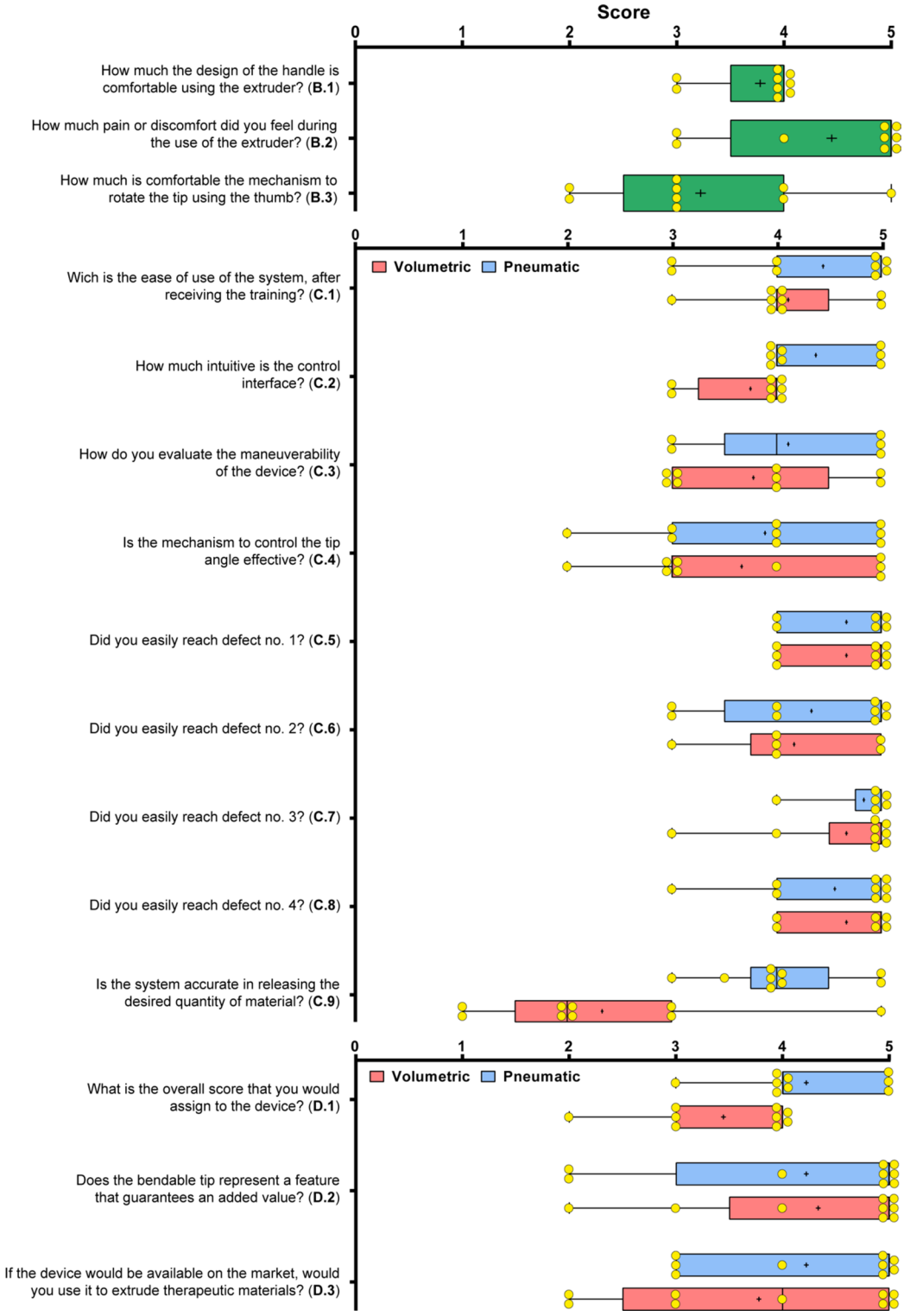

Fig. 10. Results of the questionnaire administered to the surgeons after the usability test. Data are grouped as box plots with median, minimum and maximum, yellow circles show single scores.

Also, no significant differences were found in the yield stress values. The role of the yield stress is crucial in both cell miscibility and material deposition. The incorporation of cells within the hydrogels may influence the rheological behavior of such materials. Nonetheless, the scientific literature suggests that only a relatively high cell density (larger than $1–2 \times 10^6$ cells/mL) can affect the hydrogel printability, which means accuracy in the hydrogel deposition[36,37]. For example, comparing one of the materials investigated in this study (e.g., VG-RGD) with the same including 2×10^6 cells/mL[38], no significant differences can be observed in the rheological indexes

(1.12 ± 0.36 vs. 0.88 ± 0.30 for K, 0.30 ± 0.04 vs. 0.30 ± 0.07 for n), as well as in the yield stress (0.56 ± 0.29 vs. 0.14 ± 0.06). Since the cell density considered in this work was well below the mentioned threshold, we can assume that the level of control over material extrusion would not be affected by the presence of cells Besides, testing three materials with different viscosities allowed the evaluation of the device while working in different scenarios. In fact, material viscosity plays a relevant role during material extrusion[39]. In this work, AG represented the higher viscosity example, while VG-RGD and GGMA showed a lower viscosity; they did not differ significantly.

The diameter of the extruder represents another important parameter of the device design. In the device here proposed, the nitinol tip diameter size allowed the assembly of polymeric tubes with different internal diameters. This feature would allow the selection of the best tube diameter according to the material properties. In this work, the extrusion parameters have been evaluated for three internal diameters (2.0, 1.4, and 0.5 mm). The extrusion force curves reached a plateau for the 2.0 mm and 1.4 mm sized tubes (Fig. 5). In the case of the 0.5 mm diameter, the force profiles showed an increasing trend over the displacement for GGMA and AG, letting the control of the extruded hydrogel hardly feasible. The 1.4 mm internal diameter tube was selected and preferred to the 2.0 mm for the choice of the final tube used in the arthroscope. There was no significant difference between straight and bent tip configurations for all the hydrogels extruded with a 1.4 mm tube, while for the 2.0 mm tube, there was a significant statistical difference in the extruding force for AG, probably due to partial occlusion of the tube during the bending of the tip.

The outcomes of the extrusion characterization were used to validate the estimation of the shear stress obtained through CFD simulations. Since this parameter severely influences cell viability, simulations can be helpful in verifying ideal experimental conditions. The shear stress causes the shearing deformation of materials and cells along the plane parallel to the stress direction[40]. It is directly influenced by the dispensing pressure, the tube diameter, and the material viscosity, especially when the tube diameter is decreased to enhance the printing resolution[41]. Highly viscous solutions can increase the shear stress during extrusion, leading to the rupture of the cell membrane[42]. The shear stress obtained for the AG with the intermediate tube (1.4 mm) was significantly higher than the one found in the other cases. The highest values obtained through CFD simulations are comparable with similar applications in literature[43], and well below the safety threshold of 5 kPa[44], which should ensure cell viability. In general, the shear stresses found in this study can be considered safe due to the relatively low viscosity of the hydrogels, particularly VG-RGD and GGMA. In addition, the tubes' diameters considered were larger than those used in other applications, such as the *Biopen*[13,14] or other portable bioprinters[30]. Safe values of shear stress usually contrast with high resolutions systems: larger diameters commonly decrease the risk of cell damage as well as the extrusion resolution. In this work, the resolution obtained is lower than in other extrusion-based devices[45,46]. However, the extrusion resolution found for each material can be considered acceptable for cartilage-related applications (20–50 µL for VG-RGD and ~ 70 µL for AG, Fig. 7). These values slightly increased in the case of a "fall" configuration (tip not in contact with the tissue), and there was no difference between the straight and the bent configurations. The higher viscosity of AG influenced the results in terms of extrusion time with the volumetric supply unit. This aspect was even more critical when decreasing the velocity input to 0.016 mm/s: more than 150 s were required to start releasing, which was not adequate for an arthroscopic procedure. Apart from this particular case, the released quantity of hydrogel was always in agreement with the theoretical one set on the supply unit. Comparing the supply units, the pneumatic one released a lower amount of material, up to 70% less than the volumetric one, in the "contact" configuration. The higher resolution provided by the pneumatic unit influenced the surgeons' opinion, as noticeable in the score reported in the questionnaires after the usability test on a human cadaver knee (Fig. 10). Indeed, a higher control on material release was considered a crucial aspect by the surgeons, whose preference tended towards the extruder equipped with the pneumatic supply unit.

Extrusion-based systems typically work with different supply systems to extrude the material, namely pneumatic (with or without a piston) and mechanical, based on a piston and a screw[47]. Pneumatic-based extrusion is the most widely employed strategy in tissue engineering and biofabrication[48]. Pneumatic systems exploit pressurized air to extrude the material, and they are usually preferred due to their ease of use and accuracy. A second common approach is the volumetric-based extrusion, based on the displacement-controlled movement of a piston to release a specified amount of material. Recently, the process-induced cell damages due to pneumatic and screw-driven bioprinting have been analyzed. Screw-driven bioprinting generally induces more cell damage due to the driving forces than pneumatic-based extrusion, varying with the printing conditions[41]. For these reasons, we compared the pneumatic and the volumetric-based extrusion applied through a plunger.

Cells can be considered viscoelastic particles that are sensitive to environmental variables. During extrusion, cells are forced to flow through the needle and undergo sustained mechanical forces, which can provoke localized distortions of cell membranes. Mechanical forces experienced by cells generally include tensile, compressive, shear, and/or extensional stress[49–51]. As a result, the cell membrane integrity might be compromised, reducing the possibility of keeping them alive after the extrusion procedure. A harmful effect might be induced whenever the applied pressure is high and maintained for a long period.

The biological characterization aimed at validating the clinical relevance of both supply units. Three different human chondrocyte-laden hydrogel solutions, suitable for treating cartilage, were extruded to evaluate the influence of the extrusion process on cell behavior. The viability of HCs remained high in VG-RGD, GGMA and AG hydrogels at all time points, with some morphologic differences that emerged in the case of the VG-RGD (Fig. 8). Such a different behavior was probably due to the different material chemistry of the polymeric matrices. VG-RGD is more prone to promote cell attachment and cell–matrix interactions during the cell culture in a 3D environment, due to the presence of the cell adhesive RGD peptide. Indeed, the cell metabolic activity within VG-RGD resulted in the highest values at all time points. These outcomes on VG-RGD hydrogel are in agreement with previous studies[19], although the viability of human adipose-derived stem cells (hASCs) was there considered. As it concerns the GGMA, the results are comparable to other biological evaluations performed on

light-mediated crosslinked hydrogels. In fact, the high viability of HCs at day 7 was similar to that found for hASCs[20] and for human dermal fibroblast cells[52] (with GGMA at 1% w/v). The round shape of HCs embedded into GGMA hydrogels may be due to the higher stiffness of such hydrogels after photo-crosslinking, which tended to keep cells encapsulated. Moreover, the metabolic activity slightly increased over time, even if an evident cell proliferation was absent. Finally, the outcomes found for the AG evidenced that such hydrogel did not guarantee increased cell metabolic activity, even if they remained alive over 7 days as highlighted by the Live/Dead assay. A lower concentration of calcium chloride could assist HCs in increasing their activity by decreasing the degree of reticulation of the alginate. However, our results show that the viability of HCs within each material did not differ between the extrusion units after material extrusion, proving the safety of both the volumetric and pneumatic supply units. The viability was assessed by varying the hydrogel formulation, viscosities properties and crosslinking methods (based on ions and light): these outcomes are relevant in view of a clinical translation of the device to extrude materials with different properties. The cell density investigated in this work was smaller than most commonly investigated densities, as several pre-clinical studies favored larger seeding densities (e.g., $1–2 \times 106$ chondrocytes/mL)[53]. Nonetheless, the choice of the most appropriate chondrocyte density to be used in clinical scenarios is still a matter of debate. Uncertainty in result interpretation may be caused by the multifactorial nature of cartilage repair and on the post-operative rehabilitation regimen. However, the cell density chosen in this study is comparable to other studies, in which the cartilage matrix production by cell-laden hydrogels has been demonstrated[54,55].

Involving the surgeons in the usability test and getting their opinion is a useful practice in the medical field to validate prototypes[56,57]. The ex vivo conditions provided important feedback and hints about functionality, comfort and technical aspects. The results demonstrated that the device was comfortable and allowed the operator to easily reach all cartilage defects inside the knee thanks to the bendable tip. As demonstrated by the free comments reported in Table S1, some open points on the volumetric extrusion unit and tip diameter remain, and they will be considered in future device advancements.

Despite the test on the proposed device was conducted in a dry arthroscopy scenario, this does not exclude its possible exploitation in wet arthroscopy contexts. In this framework, the chemistry of hydrogels will assume a crucial role, as they must guarantee efficient and fast crosslinking when immersed in an aqueous and saline environment, to avoid dissolution while keeping high cell viability. Photocrosslinkable hydrogels, such as the GGMA, represent suitable candidates for this application, as the hydrogel crosslinking can be accelerated by adjusting the light dose[58].

Conclusions

This work presents a novel handheld device for controlled extrusion of cell-laden hydrogels in arthroscopic treatments (e.g., for osteochondral defects, or osteoarthritis treatment). The device's bendable, disposable nitinol tip enables extrusion of cell-laden hydrogels in hard-to-reach areas of the joint, constituting an advancement in terms of arthroscopic procedures, but also in the field of in situ bioprinting. This technology has the potential to enhance the effectiveness of cartilage regeneration techniques, with a good trade-off between accuracy and invasiveness. Future efforts will be dedicated to implementing slight modifications to improve ergonomics and to guarantee full adherence to regulatory aspects, with the objective of fully exploring the potential of this tool in preclinical and clinical scenarios.

Data availability

The datasets generated during and/or analyzed during the current study are available from the corresponding author on reasonable request.

Received: 18 October 2023; Accepted: 16 August 2024
Published online: 27 August 2024

References

1. Martín, A. R., Patel, J. M., Zlotnick, H. M., Carey, J. L. & Mauck, R. L. Emerging therapies for cartilage regeneration in currently excluded "red knee" populations. *NPJ Regener. Med.* **4**, 12. https://doi.org/10.1038/s41536-019-0074-7 (2019).
2. Wu, Y. *et al.* Three-dimensional bioprinting of articular cartilage: A systematic review. *Cartilage* **12**, 76–92. https://doi.org/10.1177/1947603518809410 (2021).
3. Betancourt, N. & Chen, X. Review of extrusion-based multi-material bioprinting processes. *Bioprinting* **25**, e00189. https://doi.org/10.1016/j.bprint.2021.e00189 (2022).
4. O'Connell, C. D. *et al.* Within or without you? A perspective comparing in situ and ex situ tissue engineering strategies for articular cartilage repair. *Adv. Healthc. Mater.* **11**, e2201305. https://doi.org/10.1002/adhm.202201305 (2022).
5. Aisenbrey, E. A. *et al.* A stereolithography-based 3D printed hybrid scaffold for in situ cartilage defect repair. *Macromol. Biosci.* **18**, 1700267. https://doi.org/10.1002/mabi.201700267 (2018).
6. Samandari, M., Mostafavi, A., Quint, J., Memić, A. & Tamayol, A. In situ bioprinting: Intraoperative implementation of regenerative medicine. *Trends Biotechnol.* **40**, 1229–1247. https://doi.org/10.1016/j.tibtech.2022.03.009 (2022).
7. Mahmoudi, Z. *et al.* In situ 3D bioprinting: A promising technique in advanced biofabrication strategies. *Bioprinting* https://doi.org/10.1016/j.bprint.2023.e00260 (2023).
8. Singh, S., Choudhury, D., Yu, F., Mironov, V. & Naing, M. W. In situ bioprinting—Bioprinting from benchside to bedside?. *Acta Biomater.* **101**, 14–25. https://doi.org/10.1016/j.actbio.2019.08.045 (2020).
9. Dias, J. R. *et al.* In situ enabling approaches for tissue regeneration: Current challenges and new developments. *Front. Bioeng. Biotechnol.* **8**, 85. https://doi.org/10.3389/fbioe.2020.00085 (2020).
10. Albanna, M. *et al.* In situ bioprinting of autologous skin cells accelerates wound healing of extensive excisional full-thickness wounds. *Sci. Rep.* **9**, 1856. https://doi.org/10.1038/s41598-018-38366-w (2019).
11. Ma, K. *et al.* Application of robotic-assisted in situ 3D printing in cartilage regeneration with HAMA hydrogel: An in vivo study. *J. Adv. Res.* **23**, 123–132. https://doi.org/10.1016/j.jare.2020.01.010 (2020).

12. Li, L. *et al.* Robotic in situ 3D bio-printing technology for repairing large segmental bone defects. *J. Adv. Res.* **30**, 75–84. https://doi.org/10.1016/j.jare.2020.11.011 (2021).
13. O'Connell, C. D. *et al.* Development of the Biopen: A handheld device for surgical printing of adipose stem cells at a chondral wound site. *Biofabrication* **8**, 015019. https://doi.org/10.1088/1758-5090/8/1/015019 (2016).
14. Di Bella, C. *et al.* In situ handheld three-dimensional bioprinting for cartilage regeneration. *J. Tissue Eng. Regen. Med.* **12**, 611–621. https://doi.org/10.1002/term.2476 (2018).
15. Zhao, W., Hu, C. & Xu, T. In vivo bioprinting: Broadening the therapeutic horizon for tissue injuries. *Bioact. Mater.* **25**, 201–222. https://doi.org/10.1016/j.bioactmat.2023.01.018 (2023).
16. Hakimi, N. *et al.* Handheld skin printer: In situ formation of planar biomaterials and tissues. *Lab Chip* **18**, 1440–1451. https://doi.org/10.1039/c7lc01236e (2018).
17. Mostafavi, A. *et al.* In situ printing of scaffolds for reconstruction of bone defects. *Acta Biomater.* **127**, 313–326. https://doi.org/10.1016/j.actbio.2021.03.009 (2021).
18. Quint, J. P. *et al.* In vivo printing of nanoenabled scaffolds for the treatment of skeletal muscle injuries. *Adv. Healthc. Mater.* **10**, e2002152. https://doi.org/10.1002/adhm.202002152 (2021).
19. Manferdini, C. *et al.* RGD-functionalized hydrogel supports the chondrogenic commitment of adipose mesenchymal stromal cells. *Gels* **8**, 382 (2022).
20. Trucco, D. *et al.* Primers for the adhesion of gellan gum-based hydrogels to the cartilage: A comparative study. *Macromol. Biosci.* **22**, 2200096. https://doi.org/10.1002/mabi.202200096 (2022).
21. Denier, J. P. & Dabrowski, P. P. On the boundary-layer equations for power-law fluids. *Proc. R. Soc. Lond. Ser. A Math. Phys. Eng. Sci.* **460**, 3143–3158. https://doi.org/10.1098/rspa.2004.1349 (2004).
22. Paci, C. *et al.* Piezoelectric nanocomposite bioink and ultrasound stimulation modulate early skeletal myogenesis. *Biomater. Sci.* **10**, 5265–5283. https://doi.org/10.1039/D1BM01853A (2022).
23. https://www.karlstorz.com/gb/en/search.htm?cat=1000107520. STORZ, Karl Storz-Endoscope.
24. Ping, Z., Zhang, T., Gong, L., Zhang, C. & Zuo, S. Miniature flexible instrument with fibre Bragg grating-based triaxial force sensing for intraoperative gastric endomicroscopy. *Ann. Biomed. Eng.* **49**, 2323–2336. https://doi.org/10.1007/s10439-021-02781-4 (2021).
25. Kim, J., Kim, Y., Cho, K. J. & Kim, K. Development and preclinical trials of a novel steerable cannula for 360° arthroscopic capsular release in minimally invasive surgery. *Annual International Conference of the IEEE Engineering in Medicine and Biology Society. IEEE Engineering in Medicine and Biology Society. Annual International Conference* **2020**, 4890, https://doi.org/10.1109/embc44109.2020.9175681 (2020).
26. Dewaele, F. *et al.* A novel design for steerable instruments based on laser-cut nitinol. *Surg. Innov.* **21**, 303–311. https://doi.org/10.1177/1553350613508015 (2014).
27. Oliveira, J. T. *et al.* Gellan gum: A new biomaterial for cartilage tissue engineering applications. *J. Biomed. Mater. Res. Part A* **93A**, 852–863. https://doi.org/10.1002/jbm.a.32574 (2010).
28. Schwarz, S. *et al.* 3D printing and characterization of human nasoseptal chondrocytes laden dual crosslinked oxidized alginate–gelatin hydrogels for cartilage repair approaches. *Mater. Sci. Eng. C* **116**, 111189. https://doi.org/10.1016/j.msec.2020.111189 (2020).
29. Pazhouhnia, Z., Beheshtizadeh, N., Namini, M. S. & Lotfibakhshaiesh, N. Portable hand-held bioprinters promote in situ tissue regeneration. *Bioeng. Transl. Med.* **7**, e10307. https://doi.org/10.1002/btm2.10307 (2022).
30. Duchi, S. *et al.* Handheld co-axial bioprinting: Application to in situ surgical cartilage repair. *Sci. Rep.* **7**, 5837. https://doi.org/10.1038/s41598-017-05699-x (2017).
31. Huang, B. J., Hu, J. C. & Athanasiou, K. A. Cell-based tissue engineering strategies used in the clinical repair of articular cartilage. *Biomaterials* **98**, 1–22. https://doi.org/10.1016/j.biomaterials.2016.04.018 (2016).
32. Ye, K., Di Bella, C., Myers, D. E. & Choong, P. F. M. The osteochondral dilemma: Review of current management and future trends. *ANZ J. Surg.* **84**, 211–217. https://doi.org/10.1111/ans.12108 (2014).
33. Jaiprakash, A. *et al.* Orthopaedic surgeon attitudes towards current limitations and the potential for robotic and technological innovation in arthroscopic surgery. *J. Orthop. Surg.* **25**, 2309499016684993. https://doi.org/10.1177/2309499016684993 (2017).
34. Pelton, A. R., Berg, B. T., Saffari, P., Stebner, A. P. & Bucsek, A. N. Pre-strain and mean strain effects on the fatigue behavior of superelastic nitinol medical devices. *Shape Memory Superelast.* **8**, 64–84. https://doi.org/10.1007/s40830-022-00377-y (2022).
35. Alonso, J. M., Andrade del Olmo, J., Perez Gonzalez, R. & Saez-Martinez, V. Injectable hydrogels: From laboratory to industrialization. *Polymers* **13**, 650 (2021).
36. Gregory, T. *et al.* Rheological characterization of cell-laden alginate–gelatin hydrogels for 3D biofabrication. *J. Mech. Behav. Biomed. Mater.* **136**, 105474. https://doi.org/10.1016/j.jmbbm.2022.105474 (2022).
37. Majumder, N., Mishra, A. & Ghosh, S. Effect of varying cell densities on the rheological properties of the bioink. *Bioprinting* **28**, e00241. https://doi.org/10.1016/j.bprint.2022.e00241 (2022).
38. Ricotti, L. *et al.* Ultrasound stimulation of piezoelectric nanocomposite hydrogels boosts chondrogenic differentiation in vitro, in both a normal and inflammatory milieu. *ACS Nano* **18**, 2047–2065. https://doi.org/10.1021/acsnano.3c08738 (2024).
39. Mackay, M. E. The importance of rheological behavior in the additive manufacturing technique material extrusion. *J. Rheol.* **62**, 1549–1561. https://doi.org/10.1122/1.5037687 (2018).
40. Malekpour, A. & Chen, X. Printability and cell viability in extrusion-based bioprinting from experimental, computational, and machine learning views. *J. Funct. Biomater.* **13**, 40 (2022).
41. Ning, L. *et al.* Process-induced cell damage: Pneumatic versus screw-driven bioprinting. *Biofabrication* **12**, 025011. https://doi.org/10.1088/1758-5090/ab5f53 (2020).
42. Hull, S. M., Brunel, L. G. & Heilshorn, S. C. 3D bioprinting of cell-laden hydrogels for improved biological functionality. *Adv. Mater.* **34**, e2103691. https://doi.org/10.1002/adma.202103691 (2022).
43. Billiet, T., Gevaert, E., De Schryver, T., Cornelissen, M. & Dubruel, P. The 3D printing of gelatin methacrylamide cell-laden tissue-engineered constructs with high cell viability. *Biomaterials* **35**, 49–62. https://doi.org/10.1016/j.biomaterials.2013.09.078 (2014).
44. Blaeser, A. *et al.* Controlling shear stress in 3D bioprinting is a key factor to balance printing resolution and stem cell integrity. *Adv. Healthc. Mater.* **5**, 326–333. https://doi.org/10.1002/adhm.201500677 (2016).
45. Kyle, S., Jessop, Z. M., Al-Sabah, A. & Whitaker, I. S. "Printability" of candidate biomaterials for extrusion based 3D printing: State-of-the-art. *Adv. Healthc. Mater.* https://doi.org/10.1002/adhm.201700264 (2017).
46. Ying, G. *et al.* An open-source handheld extruder loaded with pore-forming bioink for in situ wound dressing. *Mater. Today. Bio* **8**, 100074. https://doi.org/10.1016/j.mtbio.2020.100074 (2020).
47. Tarassoli, S. P., Jessop, Z. M., Jovic, T., Hawkins, K. & Whitaker, I. S. Candidate bioinks for extrusion 3D bioprinting: A systematic review of the literature. *Front. Bioeng. Biotechnol.* **9**, 616753. https://doi.org/10.3389/fbioe.2021.616753 (2021).
48. Fisch, P., Holub, M. & Zenobi-Wong, M. Improved accuracy and precision of bioprinting through progressive cavity pump-controlled extrusion. *Biofabrication* https://doi.org/10.1088/1758-5090/abc39b (2020).
49. Ning, L., Betancourt, N., Schreyer, D. J. & Chen, X. Characterization of cell damage and proliferative ability during and after bioprinting. *ACS Biomater. Sci. Eng.* **4**, 3906–3918. https://doi.org/10.1021/acsbiomaterials.8b00714 (2018).
50. Boularaoui, S., Al Hussein, G., Khan, K. A., Christoforou, N. & Stefanini, C. An overview of extrusion-based bioprinting with a focus on induced shear stress and its effect on cell viability. *Bioprinting* **20**, e00093 (2020).
51. Lucas, L., Aravind, A., Emma, P., Christophe, M. & Edwin-Joffrey, C. Rheology, simulation and data analysis toward bioprinting cell viability awareness. *Bioprinting* **21**, e00119 (2021).

52. Sahraro, M., Barikani, M., Daemi, H. & Baei, P. Anti-fatigue, highly resilient photocrosslinkable gellan gum hydrogels reinforced by flexible nanoparticulate polyurethane multi-crosslinkers. *Int. J. Biol. Macromol.* **183**, 831–838. https://doi.org/10.1016/j.ijbiomac.2021.04.144 (2021).
53. Foldager, C. B., Gomoll, A. H., Lind, M. & Spector, M. Cell seeding densities in autologous chondrocyte implantation techniques for cartilage repair. *Cartilage* **3**, 108–117. https://doi.org/10.1177/1947603511435522 (2012).
54. Schmutzer, M. & Aszodi, A. Cell compaction influences the regenerative potential of passaged bovine articular chondrocytes in an ex vivo cartilage defect model. *J. Biosci. Bioeng.* **123**, 512–522. https://doi.org/10.1016/j.jbiosc.2016.11.002 (2017).
55. Dufour, A. *et al.* Combination of bioactive factors and IEIK13 self-assembling peptide hydrogel promotes cartilage matrix production by human nasal chondrocytes. *J. Biomed. Mater. Res. Part A* **107**, 893–903. https://doi.org/10.1002/jbm.a.36612 (2019).
56. Santos-Carreras, L., Hagen, M., Gassert, R. & Bleuler, H. Survey on surgical instrument handle design: Ergonomics and acceptance. *Surg. Innov.* **19**, 50–59. https://doi.org/10.1177/1553350611413611 (2012).
57. Doné, K., DiMartino, A., Judkins, T. N., Hallbeck, S. & Oleynikov, D. Evaluation of laparoscopic tools for usability and comfort. *Proc. Hum. Fact. Ergon. Soc. Annu. Meet.* **48**, 1359–1362 (2004).
58. Trucco, D. *et al.* Visible light-mediated cross-linking of injectable gellan gum hydrogels embedding human chondrocytes. *Carbohydr. Polym. Technol. Appl.* **6**, 100382. https://doi.org/10.1016/j.carpta.2023.100382 (2023).

Acknowledgements

This work received funding from the European Union's Horizon 2020 research and innovation program, Grant Agreement No. 814413, project ADMAIORA (*ADvanced nanocomposite MAterIals fOr in situ treatment and ultRAsound-mediated management of osteoarthritis*). The authors acknowledge Dr. Matteo Battaglini for his help during the confocal images' acquisition, and Dr. Andrea Aliperta for his help in preparing the manuscript figures.

Author contributions

L.R. and A.R. conceived and designed the study. F.R., T.M. and D.G. were the main operators of the mechanical, extrusion and resolution tests. D.T., L.V. and G.L. were responsible for the hydrogels preparation and biological tests. All the authors contributed to the interpretation of data. M.W. and T.G. developed the pneumatic system. D.G. carried out the computational simulations, wrote the manuscript and organized the ex vivo test. All the authors reviewed the manuscript. A.R. and S.Z. led the ex vivo test and L.R. secured funding for this study.

Competing interests

A portion of the work reported in this manuscript has been covered through the patent WO2022074632. The inventors are only the authors of this manuscript affiliated with the Scuola Superiore Sant'Anna, which is the owner of this patent according to the protection and valorization of the intellectual property agreement.

Additional information

Supplementary Information The online version contains supplementary material available at https://doi.org/10.1038/s41598-024-70426-2.

Correspondence and requests for materials should be addressed to D.G.